Mon. Not. R. Astron. Soc. **000**, 000–000 (0000) Printed 2 February 2008 (MN LATEX style file v2.2)

arXiv:astro-ph/0308352v1 20 Aug 2003

Thermal conduction and reduced cooling flows in galaxy clusters

L.M. Voigt and A.C. Fabian
Institute of Astronomy, Madingley Road, Cambridge CB3 0HA

2 February 2008

ABSTRACT
Conduction may play an important role in reducing cooling flows in galaxy clusters. We analyse a sample of sixteen objects using *Chandra* data and find that a balance between conduction and cooling can exist in the hotter clusters ($T \gtrsim 5$ keV), provided the plasma conductivity is close to the unhindered Spitzer value. In the absence of any additional heat sources, a reduced mass inflow must develop in the cooler objects in the sample. We fit cooling flow models to deprojected data and compare the spectral mass deposition rates found to the values required to account for the excess luminosity, assuming Spitzer-rate heat transfer over the observed temperature gradients. The mass inflow rates found are lower than is necessary to maintain energy balance in at least five clusters. However, emission from cooling gas may be partially absorbed. We also compute the flux supplied by turbulent heat transport (Cho et al. 2003) and find conductivity profiles which follow a strikingly similar temperature dependence to the conductivity values required to prevent cooling. Finally, we show that the cluster radio luminosities vary by over five orders of magnitude in objects with X-ray luminosities differing by no more than a factor of a few. This suggests that there is unlikely to be a straightforward correlation between the mechanical power provided by the radio lobes and the rate of energy loss in cooling flow clusters.

Key words: galaxies: clusters – cooling flows – X-rays: galaxies – conduction

1 INTRODUCTION

High resolution observations of cooling flow clusters with *XMM-Newton* and *Chandra* show no evidence for the large amounts of multiphase gas expected in the inner regions of these objects (Peterson et al. 2001; Tamura et al. 2001; Kaastra et al. 2001; Peterson 2002). Several solutions have been proposed to account for the lack of soft X-ray emission; including models which preserve the classic mass deposition rates by invoking differential absorption, mixing or inhomogeneous metallicity distributions (Fabian et al. 2001; Morris & Fabian 2002; Fabian et al. 2002a), and those which prevent, or significantly reduce, mass dropout by balancing the radiative losses by some heat source (Bertschinger & Meiksin 1986, Tucker & Rosner 1983; Churazov et al. 2001; Brüggen & Kaiser 2001).

Here we discuss the role played by conduction in transporting heat from the hot gas reservoir outside the cooling radius towards the centre of the cluster. Narayan & Medvedev (2001), Gruzinov (2002) and Fabian et al. (2002b) have shown that conduction provides heat fluxes which are close to those required to stem cooling, assuming the plasma conductivity is within an order of magnitude of the Spitzer value, $\kappa_{\rm S}$ (Spitzer 1962). The actual value for the suppression of cluster conductivity below $\kappa_{\rm S}$ remains an open question, and depends on detailed understanding of cluster magnetic fields. Churazov (2001) estimated the suppression factor to be ~ 0.01, whereas Narayan & Medvedev (2001) argue that it could be as high as 0.3. If the former scenario were true we could rule out conduction as a successful heating mechanism. However, recent support for heat transfer rates close to the Spitzer rate means that conduction may have a significant effect on cluster evolution.

In order to test the conduction hypothesis further, detailed spatial analyses of individual clusters have been carried out by Voigt et al. (2002) and Zakamska & Narayan (2002). In the latter study, a simple model in which conduction balances cooling was used to generate theoretical temperature and density profiles. The conductivity values required to produce profiles which were reasonable fits ‘by eye’ to the observed profiles were then used to assess whether or not conduction can be effective. Zakamska & Narayan concluded that half the clusters in their sample could be prevented from cooling if conduction is operating at a rate between (0.1–0.4) $\kappa_{\rm S}$. They suggest that the remaining clusters are heated by the central radio source.

Voigt et al. (2002) calculated the conductivity required to replace heat loss as a function of radius using the observed temperature and density profiles of Abell 1835 (Schmidt et al. 2001) and Abell 2199 (Johnstone et al. 2002). We found that whilst conduction at the Spitzer rate was able to prevent cooling in the outer parts of the cooling flow region, a factor of 2 or more above the Spitzer rate was required in the very centre (within about 20 kpc). We suggested that conduction suppresses cooling, and that in some cases this suppression is complete, and in others partial. In the latter case a reduced cooling flow develops. In this paper we extend the work of Voigt et al. (2002) to a sample of sixteen galaxy clusters using archival *Chandra* data. In clusters where the required conductivity is above the Spitzer value we fit cooling flow models to the spectra and compare the mass deposition rates found to those required to maintain energy balance with conduction at $\kappa_{\rm S}$.

We consider the possibility that heat is transported by turbulent diffusion in Section 7.

Throughout the paper we assume a cosmology with H_0=71 $\rm km\,s^{-1}\ Mpc^{-1}$, Λ=0.73 and $\Omega_{\rm m}$=0.27.

2 CLUSTERS AND DATA REDUCTION

The clusters in our sample are listed in Table 1 and include objects ranging in redshift from 0.0–0.5 and in temperature from $\sim$ 2–15 keV. The clusters were observed using chip 7 on the ACIS-S detector on board *Chandra*, allowing spatially-resolved analysis of the cooling flow region. In each case the data were reduced using the CIAO (*Chandra Interactive Analysis of Observations*) software package. We used the Markevitch script (LC_CLEAN) to remove flares and strong point sources were identified by eye and subtracted from the regions files. ACIS 'blank-sky' datasets were used to subtract the background. Ancillary-response and response matrices were produced using the CIAO MKWARF and CIAO MKRMF programs and data were binned to have at least 20 counts per PHA channel.

Spectra were extracted in the 0.5–7.0 keV energy range in circular annuli around the X-ray emission peak. The following regions were excluded from the cluster images: strong central sources in PKS 1404–267, Hydra A and 3C 295; enhanced, hot emission south–east of the X–ray centre in RXJ 1347.5-1145; emission interior to the radio jets in Cygnus A; X–ray holes in Hydra A and hot emission 180–280 kpc north of the centre in Abell 478. A detailed analysis of the temperature and density profiles of the sample will be given in future work (Voigt et al. 2003, in prep.).

3 SPECTRAL MODEL AND TEMPERATURE AND EMISSION MEASURE PROFILES

Deprojected temperature and emission measure profiles were found for each cluster assuming spherically symmetric emission from shells of single phase gas. The spectra were fitted in XSPEC (Arnaud 1996) with the MEKAL (Mewe et al. 1985; Liedahl et al. 1995) plasma emission code, absorbed by the PHABS (Balucinska-Church & McCammon 1992) photoelectric absorption code. Deprojection was performed using the PROJCT routine. The elements were assumed to be present in the Solar ratios measured by Anders & Grevesse (1989) and the abundance allowed to vary between shells. The Galactic absorption column density was left as a free parameter in the fits, although linked between shells. Fixing $N_{\rm H}$ at the value expected along the line-of-sight to the cluster would lead to spurious results since the counts are uncertain below $\sim$ 1 keV due to the low energy quantum efficiency degradation of the detector since launch. We do not apply the tools provided to correct for this loss in effective area (ACISABS or CORRARF) since they appear to over-correct the data, reducing the best-fitting absorption column density to zero in many objects. (We note that this over-correction is also found by Takizawa et al. (2003) in an analysis of Abell 3112). We therefore allow an artificially high absorption column to account for the loss in low energy counts since the reduction in effective area is similar in shape to the subtraction of counts by a foreground screen. We stress that the temperature profiles obtained are the same within the 1σ error bars both with and without the correction to the low energy counts when $N_{\rm H}$ is left as a free parameter in the fits. We are therefore confident that the results are robust. The best-fitting $N_{\rm H}$ values and reduced chi-squares of the fits are shown in Table 2 (model A).

The temperature profiles obtained are shown for the whole sample in Fig. 7. The one sided error bars plotted (necessary for chi-square calculations) are the root-mean-square of the two sided 1σ uncertainties found using the error command in XSPEC .

4 CALCULATION OF THE EFFECTIVE CONDUCTIVITY

4.1 Energy equations

The luminosity emitted from an isothermal plasma of density n, temperature T and metallicity Z per unit volume is given by

$$L = n^2\Lambda(T,Z) \tag{1}$$

where $\Lambda(T,Z)$ is the cooling function for a plasma losing energy by bremsstrahlung radiation and line emission.

Assuming the shells contain single phase gas, we can write the total luminosity emitted from shell j with volume ΔV_j as

$$\Delta L_j^{\rm tot} = EM_j\Lambda(T_j,Z_j) \tag{2}$$

where $EM_j = n_j^2\Delta V_j$ is the emission measure of the shell.

The net heat transferred to the $j^{\rm th}$ shell by conduction is given by

$$\Delta L_j^{\rm cond} = 4\pi r_j^2\kappa_j\left(\frac{dT}{dr}\right)_j - 4\pi r_{j-1}^2\kappa_{j-1}\left(\frac{dT}{dr}\right)_{j-1} \tag{3}$$

where $({\rm d}T/{\rm d}r)_j$ is the temperature gradient and κ_j the plasma conductivity across the outer boundary of the $j^{\rm th}$ shell.

We calculate the conductivity required to prevent cooling in the $j^{\rm th}$ shell by equating Equations 2 and 3 and summing from the centre of the cluster outwards

$$4\pi r_j^2\kappa_j^{\rm eff}\left(\frac{dT}{dr}\right)_j = \sum_{i=1}^{j} EM_j\Lambda_j \tag{4}$$

where $\kappa^{\rm eff}$ is referred to as the effective thermal conductivity.

4.2 $\kappa^{\rm eff}$ calculation

The effective conductivity at the outer boundary of each shell was calculated using Equation 4. We fit power-law models to temperature profiles where the error bars overlap (see Table 3). The effective conductivity values and their 1σ uncertainties, shown for each cluster individually in Fig. 8, were determined using Monte Carlo simulations. The gas cooling times, $t^{\rm cool}$, within each shell are also plotted in Fig. 8.

We calculate $t^{\rm cool}$ using the formula

$$t^{\rm cool} \approx \frac{\frac{3}{2}nkT}{\epsilon} \tag{5}$$

Cluster	Redshift z	Obs. date	Exps. time (ks)	GTI (ks)	X-ray peak (J2000) RA Dec	d_{L} (Mpc)	d_{A} (kpc/$''$)	Refs.
2A 0335+096	0.0347	2000 Sep 06	20.0	18.1	(03 38 40.5) (+09 58 11.6)	140.6	0.7	[1]
A478	0.0880	2001 Jan 27	42.9	38.9	(04 13 25.4) (+10 27 57.1)	396.9	1.6	[2],[3]
PKS 0745-191	0.1028	2001 Jun 16	17.9	14.6	(07 47 31.2) (-19 17 38.8)	468.5	1.9	[4],[5]
Hydra A	0.0520	1999 Nov 02	24.1	17.3	(09 18 05.7) (-12 05 43.3)	228.5	1.0	[6],[7]
M87†	0.0043	2000 Jul 29	38.2	33.7	(12 30 49.4) (+12 23 28.0)	18.2	0.1	[8],[9],[10],[11]
RXJ 1347.5-1145	0.4510	2000 Apr 29	10.1	7.2	(13 47 30.7) (-11 45 09.5)	2492.9	5.7	[12],[13]
A1795	0.0632	2000 Mar 21	19.7	15.6	(13 48 52.5) (+26 35 37.8)	280.0	1.2	[14],[15]
A1835	0.2523	1999 Dec 11	19.8	18.9	(14 01 02.0) (+02 52 39.7)	1262.4	3.9	[16]
PKS 1404-267	0.0226	2001 Jun 07	7.3	6.0	(14 07 29.8) (-27 01 04.2)	97.1	0.5	[17]
3C 295	0.4605	1999 Aug 30	19.0	14.3	(14 11 20.5) (+52 12 10.5)	2556.0	5.8	[18]
A2029	0.0767	2000 Apr 12	19.9	19.8	(15 10 56.1) (+05 44 40.6)	343.2	1.1	[19]
RXJ 1532.9+3021	0.3615	2001 Aug 26	9.5	6.2	(15 32 53.8) (+30 21 00.2)	1916.3	5.0	–
Cygnus A	0.0562	2000 May 21	35.2	33.3	(19 59 28.3) (+40 44 02.0)	247.7	1.1	[20]
A2390	0.2301	2000 Oct 08	10.0	7.4	(21 53 36.8) (+17 41 44.1)	1136.8	3.6	[21],[13]
Sersic 159-03 (AS 1101)	0.0564	2001 Aug 13	10.1	9.8	(23 13 58.5) (-42 43 34.5)	248.7	1.1	[22]
A2597	0.0830	2000 Jul 28	39.9	21.3	(23 25 19.8) (-12 07 27.6)	362.3	1.5	[23]

Table 1. Properties of the sample. Redshift, observation date, exposure time, good time interval after data reduction, X-ray emission peak, luminosity distance and angular scale. † The M87 data used in this paper were taken from Di Matteo et al. (2003). Previous papers covering the X-ray spectra of these objects include: [1] Mazzotta et al. 2003; [2] Johnstone et al. 1992; [3] Sun et al. 2002; [4] De Grandi & Molendi 1999; [5] Hicks et al. 2002; [6] David et al. 2001; [7] McNamara et al. 2000; [8] Matsushita et al. 2002; [9] Molendi 2002; [10] Böhringer et al. 2001; [11] Young et al. 2002; [12] Allen et al. 2002; [13] Ettori et al. 2001; [14] Ettori et al. 2002; [15] Tamura et al. 2001; [16] Schmidt et al. 2001; [17] Johnstone et al. 1998; [18] Allen at al. 2001b; [19] Lewis et al. 2002; [20] Smith et al. 2002; [21] Allen at al. 2001a; [22] Kaastra et al. 2001; [23] McNamara et al. 2001.

Cluster	Model A PROJCT*PHABS(MEKAL) χ^2/dof	Model A Fitted N_{H} (10^{20} cm^{-2})	Model B PROJCT*PHABS(MEKAL+MKCFLOW) χ^2/dof	Model B Fitted N_{H} (10^{20} cm^{-2})	F-test probability B → A	Galactic N_{H} (10^{20} cm^{-2})
2A 0335+096	2227.300/1404	27.06±0.20	1888.495/1400	28.78±0.23	0.00	17.8
A478	3370.693/2654	32.72±0.17	3299.203/2649	33.54±0.20	5.5×10^{-11}	15.2
PKS 0745-191	2468.181/2193	40.73±0.35	2409.976/2187	43.14±0.43	1.7×10^{-9}	42.4
Hydra A	1429.901/1352	3.67±0.19	1418.988/1346	3.77±0.20	0.11	4.90
M87	3171/1271	1.97±0.12	–	–	–	2.5
RXJ 1347.5-1145	317.3776/312	6.63±0.72	317.2172/309	6.72±0.90	0.98	4.85
A1795	1753.311/1491	1.43±0.13	1706.515/1489	1.69±0.14	1.8×10^{-9}	1.19
A1835	1306.118/1291	2.94±0.24	1305.088/1288	3.00±0.27	0.78	2.32
PKS 1404-267	670.9301/625	10.06±0.50	649.8231/597	10.03±0.52	0.88	4.52
3C 295	133.3785/137	2.49±1.12	133.0522/135	2.62±1.45	0.85	1.33
A2029	2779.268/2472	3.81±0.12	2751.292/2466	4.02±0.13	3.5×10^{-4}	3.05
RXJ 1532.9+3021	314.4362/322	5.71±0.68	309.5464/319	7.04±1.18	0.17	2.16
Cygnus A	1412.082/1237	30.29±0.32	1411.647/1235	30.42±0.34	0.83	34.8
A2390	589.6790/617	11.12±0.53	576.4204/615	12.47±0.62	9.2×10^{-4}	6.80
Sersic 159-03	867.0667/802	6.31±0.41	843.1426/798	6.60±0.43	1.7×10^{-4}	1.79
A2597	1396.950/1222	3.24±0.22	1337.056/1216	3.88±0.24	9.9×10^{-10}	2.49

Table 2. Chi-squares and best-fitting N_{H} values for models A and B. The F-test probability that model B provides a better representation of the data than model A, and the galactic absorption column along the line-of-sight to the cluster (from Dickey & Lockman 1990) are also tabulated.

where ϵ is the total emissivity and n is the total number density of particles.

Since $\epsilon \Delta V = EM\Lambda = n_{\mathrm{e}} n_{\mathrm{h}} \Delta V \Lambda$, and using $n \approx 2n_{\mathrm{e}}$ and $n_{\mathrm{e}} \approx (6/5) n_{\mathrm{h}}$, then $\epsilon \approx (5/6) n_{\mathrm{e}}^2 \Lambda$, where n_{e} and n_{h} are the electron and hydrogen number densities respectively. Substituting into Equation 5 we have the following expression for the cooling time of gas in the j^{th} shell

$$t_j^{\mathrm{cool}} \approx 3.3 \frac{kT_j}{(EM_j/\Delta V_j)^{\frac{1}{2}} \Lambda_j}. \qquad (6)$$

The cooling time profiles (which are mostly $\propto T^{\frac{1}{2}} n^{-1}$) are plotted for the whole sample in Fig. 1. They closely track the same radial-dependence curve (a similar result is found for the entropy profiles $\propto T n^{-\frac{2}{3}}$). We find no trend in terms of 'old' or 'young' cooling flows which would indicate cyclic heating behaviour.

We define the cooling radius as where the cooling time of the gas drops to 5 Gyr.

Cluster	a	b	χ^2/dof
PKS 0745-191	1.18	0.38	11.83/7
Hydra A	1.72	0.18	5.39/6
RXJ 1347.5-1145	2.84	0.31	1.21/2
A1795	1.68	0.26	6.09/3
A1835	1.58	0.34	2.86/5
PKS 1404-267	0.73	0.22	1.93/5
3C 295	1.91	0.17	0.43/2
A2029	2.43	0.24	11.86/7
RXJ 1532.9+3021	0.83	0.43	0.08/2
Cygnus A	1.34	0.36	0.99/2
A2390	2.06	0.27	1.34/3
Sersic 159-03	1.21	0.16	4.90/5
A2597	1.00	0.33	13.42/5

Table 3. The parameters and reduced chi-square values for the best-fitting power laws ($T = ar^b$) to the temperature profiles. A power law is not required for clusters where the error bars are small (M87, 2A 0335+096 and Abell 478).

5 THERMAL CONDUCTION

5.1 Spitzer conductivity

The conductivity of a hydrogen plasma completely free from magnetic fields was derived by Spitzer (1962)

$$\kappa_{\rm S} = \frac{1.84 \times 10^{-5} T^{\frac{5}{2}}}{\ln \Lambda}\,{\rm erg\,s^{-1}\,cm^{-1}\,K^{-1}} \qquad (7)$$

where $\ln \Lambda$ is the Coulomb logarithm (ratio of the largest to the smallest impact parameter)

$$\ln \Lambda = 37.8 + \ln \left[\left(\frac{T}{10^8\ {\rm K}} \right) \left(\frac{n_{\rm e}}{10^{-3}\ {\rm cm}^{-3}} \right)^{-\frac{1}{2}} \right]. \qquad (8)$$

This term depends only weakly on on the plasma temperature and density and so we can re-write this equation as

$$\kappa_{\rm S} \simeq \kappa_0 T^{\frac{5}{2}} \qquad (9)$$

where $\kappa_0 \simeq 5.0 \times 10^{-7}$ erg s^{-1} cm^{-1} K$^{-\frac{7}{2}}$ for electron densities and temperatures appropriate to the objects considered.

5.2 Magnetic field effects

The presence of magnetic fields in the intracluster medium will reduce the conductivity below the full Spitzer rate, such that $\kappa = f\kappa_{\rm S}$, where $f \leq 1$. The gyroradius of charged particles around magnetic field lines in the intracluster plasma, r_g, is much less than the mean free path of charged particles due to collisions, λ_e. The effective mean free path will be reduced by a factor $\sim r_g^2/\lambda_e$ perpendicular to ordered magnetic field lines. Assuming a radial temperature gradient, $f \sim 0.3$ for a radial magnetic field and negligible for a circumferential field.

However, observations show that the magnetic fields may be tangled (Carilli & Taylor 2002). The conductivity then depends on the coherence length of the magnetic field. The theory was first discussed by Rechester & Rosenbluth (1978) and later developed by Chandran & Cowley (1998). These initial studies predicted a suppression factor $f \sim$ 0.01–0.001. More recently, Narayan & Medvedev (2001) have suggested that a magnetic field which is chaotic over a wide range of scales will lead to a suppression factor in the range $\sim$ 0.1–0.4. Maron, Chandran & Blackman (2003), on the other hand, support a value $\sim$ 0.02.

We note that heat conduction at close to the Spitzer rate is observed in the Solar wind when the electron mean free path is small compared with the temperature gradient (Salem et al. 2003).

The conductive heat flux will be overestimated in the outer regions of clusters if the mean free path of electrons is comparable to or greater than the scale length of the temperature gradient (Cowie & McKee 1977). ‘Saturation’ of the conductivity at large radii may explain why significant amounts of heat will not be removed from the cluster outwards (Loeb et al. 2002 suggested that conduction at the Spitzer rate throughout galaxy clusters would result in significant amounts of thermal energy being leaked to the surrounding intercluster medium). Also, fields lines may be stretched out radially by mass inflow, resulting in Spitzer rate conduction being restricted to cluster centres (Bregman & David 1988; Fabian et al. 2002b).

6 ANALYSIS

6.1 Effective conductivity profiles

The effective conductivity profiles are plotted out to the cooling radius for the whole sample in Fig. 1. We find that when the temperature of the cluster drops below ∼5 keV, conductivity values above the Spitzer curve are required. This demonstrates the strong dependence of thermal heat transport on temperature and suggests that even Spitzer-rate conduction will be unable to prevent cooling in low temperature clusters.

Studying the individual effective conductivity profiles shown in Fig. 8 in detail, we find that in four clusters (Abell 1795, Abell 2029, Cygnus A and Abell 2390) conduction at or below the Spitzer rate would prevent cooling from taking place everywhere inside the cooling radius. The remaining clusters in the sample require the plasma conductivity to be greater than $\kappa_{\rm S}$ in at least one shell. (We note that in studies by Fabian et al. (2002) and Medvedev et al. (2003), where the conductivity required to prevent cooling is calculated at the cooling radius only, clusters such as RXJ 1532.9+3021 and 3C 295 would appear below the Spitzer curve. Detailed studies of the temperature profiles right into the centres of clusters are therefore needed to accurately assess the energetic feasibility of conduction over the entire cooling flow region).

The conductivity values required to prevent cooling at radial positions within the cluster where the cooling time of the gas is 13, 5 and 1 Gyr are shown in Table 4 as a fraction of $\kappa_{\rm S}$. Conduction may stop large mass inflows from taking place in the outer parts of the cooling flow region, but will be unable to prevent a net heat loss in the inner regions of the majority of objects in the sample. Since most of the implied mass deposition takes place at larger radii, the small mass inflows which must develop in the centre (in the absence of any additional heat sources) may be below the spectral constraints imposed by recent observations.

6.2 Conduction + reduced cooling flow?

For clusters in which conductive heat transfer is insufficient to prevent cooling, we calculate the rate at which mass must drop out in each shell, assuming conduction is operating at the Spitzer rate over the observed temperature gradients. This provides lower limits on the mass deposition rates required, since the plasma conductivity is reduced by a factor $f \leq 1$ in the presence of magnetic fields.

Cluster	Cooling time (Gyr)	Temperature (keV)	$\kappa^{\rm eff}$ ($/\kappa_{\rm S}$)	$\dot{M}^{\rm clas}$ ($\mathrm{M}_{\odot}$ yr^{-1})	$\dot{M}^{\rm spec}$ ($\mathrm{M}_{\odot}$ yr^{-1})
2A 0335+096	13.7	–	–		
	5.0	3.2	0.8	377±8	80±5
	1.0	2.2	**2.8**		
A478	13.7				
	5.0	6.6	0.3	892±22	$112\pm^{22}_{19}$
	1.0	4.5	0.2		
PKS 0745-191	13.7	9.5	0.1		
	5.0	7.6	0.3	1269±30	$317\pm^{35}_{29}$
	1.0	5.1	1.0		
Hydra A	13.7	–	–		
	5.0	3.9	1.0	239±7	$8\pm^{6}_{4}$
	1.0	3.2	**1.8**		
RXJ 1347.5-1145	13.7	–	–		
	5.0	14.4	0.1	3518±304	$75\pm^{743}_{72}$
	1.0	10.5	0.5		
A1795	13.7	–	–		
	5.0	5.4	0.4	268±6	$30\pm^{5}_{5}$
	1.0	4.1	0.6		
A1835	13.7	10.5	0.1		
	5.0	8.3	0.3	1453±64	$34\pm^{43}_{34}$
	1.0	6.4	0.9		
PKS 1404-267	13.7	–	–		
	5.0	1.8	**2.0**	54±4	5±1
	1.0	1.4	**3.9**		
3C 295	13.7	4.8	1.1		
	5.0	4.5	**1.7**	632±83	$16\pm^{230}_{12}$
	1.0	3.9	**3.2**		
A2029	13.7	8.7	0.1		
	5.0	7.5	0.2	453±12	$30\pm^{10}_{13}$
	1.0	5.2	0.4		
RXJ 1532.9+3021	13.7	–	–		
	5.0	7.5	0.4	2375±169	$592\pm^{357}_{260}$
	1.0	4.9	**1.5**		
A2390	13.7	8.9	0.1		
	5.0	7.7	0.2	765±76	$339\pm^{42}_{118}$
	1.0	–	–		
Sersic 159-03	13.7	2.7	**2.3**		
	5.0	2.5	**4.1**	245±13	$33\pm^{11}_{9}$
	1.0	2.1	**6.2**		
A2597	13.7	–	–		
	5.0	4.5	0.5	409±14	$57\pm^{14}_{13}$
	1.0	3.1	**1.5**		

Table 4. Effective conductivity values (shown in bold where $\kappa^{\rm eff} > \kappa_{\rm S}$) and temperatures at radial positions corresponding to cooling times of 13.7, 5 and 1 Gyr. The integrated classic and spectrally-determined mass deposition rates within the cooling radius are shown. M87 and Cygnus A are not included in this table since the analysis of these clusters does not extend over the entire cooling flow region. Data are unavailable (shown by dashed lines) either when the inner region is unresolved or the relevant cluster emission lies outside the chip boundary.

We then compare these values with spectral mass deposition rates, determined by fitting cooling flow models to the spectra.

We note that for any blobs of cool gas to exist, conduction of heat to the blobs must be highly suppressed. This probably requires them to be separate magnetic structures.

6.2.1 *Inhomogeneous cooling flows*

The observed bolometric luminosity from a single shell j in a spherically symmetric, inhomogeneous, steady state, subsonic cooling flow is given by

$$\Delta L_j^{\rm tot} - \Delta L_j^{\rm cond} = \Delta \dot{M}_j H_j + \delta_j \Delta \dot{M}_j \Delta\Phi_j + \dot{M}_{j-1}\left(\Delta H_j + \Delta\Phi_j\right) \tag{10}$$

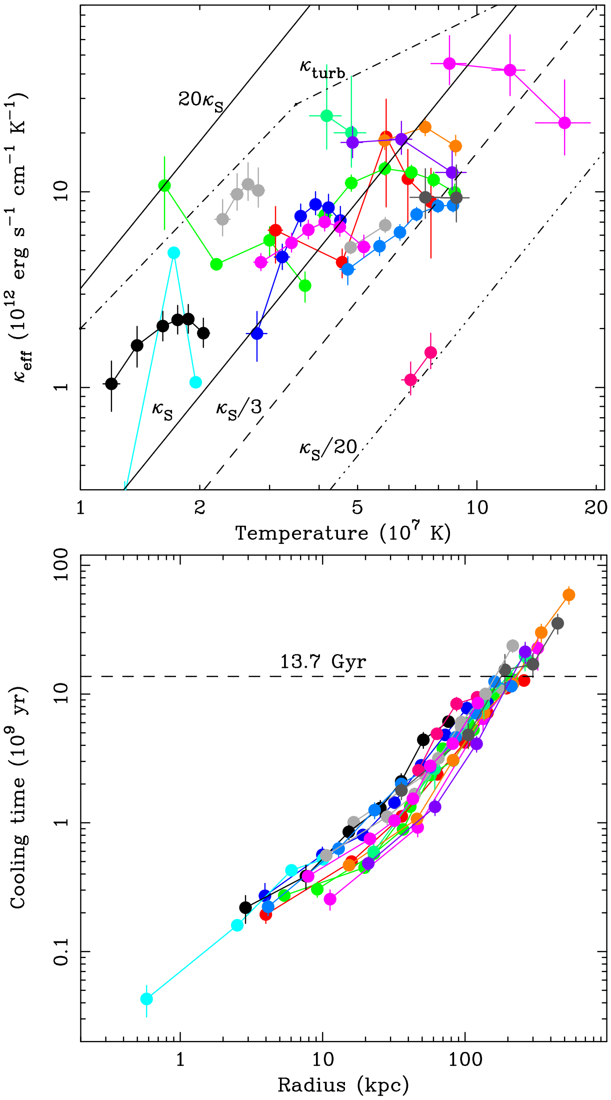

Figure 1. Effective conductivity profiles (upper plot) and cooling times (lower plot) for the sample. $\kappa_{\rm S}$ is the Spitzer conductivity and $\kappa_{\rm turb}$ is the turbulent conductivity. Note that $\kappa_{\rm turb}$ is calculated at a fixed cooling time (1 Gyr).

where $\Delta\dot{M}_j$ is the rate at which mass is deposited in the $j^{\rm th}$ shell and $\dot{M}_{j-1}$ is the rate at which mass flows through the shell towards the centre, such that

$$\dot{M}_j = \sum_{i=1}^{j} \Delta\dot{M}_i \qquad (11)$$

H_j, ΔH_j, $\Delta\Phi_j$ are the enthalpy of the ambient gas in the $j^{\rm th}$ shell and the enthalpy change and gravitational potential difference across it. δ_j is a factor of order unity which takes into account the fact that gas is deposited throughout the volume of the shell (see e.g. Fabian et al. 1985).

The first term represents the luminosity emitted by gas cooling out of the flow. Since the flow rate is long compared with the cooling rate, the gas can be assumed to be cooling out at a fixed radius and therefore, under the condition of hydrostatic equilibrium, at constant pressure. The spectrum emitted by a perfect gas cooling isobarically is described by Johnstone et al. (1992)

$$\Delta L_j^{\rm cool}(\nu) = \frac{5k}{2\mu m_{\rm H}}\Delta\dot{M}_j \int_0^{T_j} \frac{\epsilon_j(\nu)}{\Lambda(T)}{\rm d}T \qquad (12)$$

where $\epsilon_j(\nu)$ is the emissivity at frequency ν_j.

The second and fourth terms represent the gravitational potential energy released due to gas cooling out and gas flowing across the shell respectively. The third term is the contribution from the enthalpy change of gas flowing across the shell. The contribution from these terms to the total luminosity emitted may be comparable to that from the first term (Fabian 1994).

We note that in the classic cooling flow scenario cool gas clouds deposited out of the flow are assumed to be supported against gravitational infall. Magnetic fields were invoked to prevent clouds from falling towards the cluster centre (Fabian 1994). Fabian (2003a) discusses the possibility that blobs of gas fall inwards, giving up their gravitational potential energy to the surrounding medium as they descend through the core. The energetics show that this process could be important in the outer parts of the cooling flow region.

6.2.2 *Mass deposition rates with and without conduction*

We first calculate the mass deposition rate expected in each shell assuming the plasma conductivity is zero (i.e. $\Delta L_j^{\rm cond} = 0$); this is the classic mass deposition rate, $\Delta\dot{M}_j^{\rm clas}$.

$$\Delta L_j^{\rm tot} = \frac{5k}{2\mu m_{\rm H}}\Delta\dot{M}_j^{\rm clas}T_j \qquad (13)$$

where we have neglected the contributions from the last three terms in Equation 10.

We then calculate the mass which must cool out of the flow assuming conductive heat transfer at the Spitzer rate over the observed temperature gradients. We refer to this as $\Delta\dot{M}_j^{\rm cool}$, given by

$$\Delta L_j^{\rm tot} - \Delta L_j^{\rm cond} = \frac{5k}{2\mu m_{\rm H}}\Delta\dot{M}_j^{\rm cool}T_j \qquad (14)$$

where we put $\kappa_j = \kappa_0 T_j^{\frac{5}{2}}$ in Equation 3.

6.2.3 *Spectral mass deposition rates*

We compare the values calculated for $\Delta\dot{M}_j^{\rm cool}$ with spectral mass deposition rates, determined by fitting a cooling flow models to the data. The emission from each shell is represented by an isothermal component (plasma maintained at a constant temperature) plus a cooling flow component. The cooling term is fitted with an MKCFLOW spectrum (see Equation 12) and the isothermal term by a single MEKAL component. Since we receive projected X-ray emission, the model MKCFLOW + MEKAL is fitted to the deprojected emission from each shell. As with model A, this is carried out using the PROJCT routine. NB The MEKAL component is not there to account for emission from material outside the cooling radius and any cooling flow component detected is not a projection effect (assuming spherical symmetry), as suggested by Molendi & Pizzolato 2001. The temperatures and abundances in MKCFLOW are tied to the MEKAL values within each shell. The spectral mass deposition rate, $\Delta\dot{M}_j^{\rm spec}$, in each shell is the normalization of the

MKCFLOW component. The cooling flow model is fit to shells only where the cooling time of the gas is less than or equal to 5 Gyr. As before, the Galactic absorption column is left as a free parameter in the fits (although linked between shells) and the abundances are untied. We note that the spectral mass deposition rates obtained are statistically equivalent both with and without the CORRARF correction.

The best-fitting $N_{\rm H}$ values and reduced chi-squares for the fits are tabulated in Table 2 (model B), together with the F-test probabilities that the isothermal model provides a better representation of the data than the cooling flow model. The probabilities suggest that adding a cooling flow component to each shell provides a significantly better fit to the data for the majority of objects in the sample. For 3C 295, Abell 1835, RXJ 1347.5+1145, PKS 1404-267 and Cygnus A an additional cooling flow component is not required statistically. There is no relation between the requirement for a cooling flow component and the need for super-Spitzer plasma conductivity.

6.2.4 *Comparison between predicted and spectrally-determined mass deposition rates*

In Fig. 2 we plot the classic mass deposition rates, $\Delta\dot{M}_j^{\rm clas}$, the mass deposition rates required assuming conduction at the Spitzer rate, $\Delta\dot{M}_j^{\rm cool}$, and the spectral mass deposition rates, $\Delta\dot{M}_j^{\rm spec}$, for clusters where the effective conductivity is above the Spitzer rate.

In five clusters the spectral mass deposition rates are approximately a factor of two lower than is required for energy balance, even when $\Delta\dot{M}_j^{\rm cool}$ is halved to take into account the gravitational work done on the gas and the enthalpy released by the gas as it flows across the shell.

For clusters which have also been studied by Peterson et al. (2002), we plot $\Delta\dot{M}_j^{\rm cool}$ and $\Delta\dot{M}_j^{\rm spec}$ summed out to the cooling radius (see Fig. 3), together with the RGS upper limits or detections of cool gas within the radius shown by the dashed line. For Abell 1835 and Sersic 159-03 the spectral mass deposition rates found in this study are consistent with the RGS upper limits. There is some discrepancy between the Chandra and RGS data for Hydra A and 2A 0335+096, with a larger mass deposition rate found in this study for 2A 0335+096, and a smaller one for Hydra A.

6.2.5 *Conclusions*

Conduction at the Spitzer rate, together with a reduced, unabsorbed cooling flow equal to the spectral mass deposition rates found here is unable to account for the entire cooling luminosity in at least five clusters (Hydra A, Sersic 159-03, 2A 0335+096, Abell 1835 and PKS1404-267). Conduction at a lower rate will fail to prevent cooling in even more clusters.

Unhindered conduction is, however, able to *reduce* the mass deposition rates required for a steady-state energy balance by a significant factor (2–3 in most clusters) and the addition of a modest amount of intrinsic absorption may bring the spectral mass deposition rates into agreement with what is required. (We note too that the Chandra detector contamination, affecting counts at low energies, places an instrumental limitation on the accuracy of soft X-ray emission measurements).

As a final comment on reduced cooling flows, we plot in Fig. 4 the predicted classic and observed spectral mass deposition rates obtained for the whole sample (tabulated in Table 4). The observed values do not assume any conduction or excess absorption. We find that $\dot{M}^{\rm spec} \sim 0.1\dot{M}^{\rm clas}$. This correlation indicates that there is no relation between the spectral mass deposition rates found and the effective conductivity.

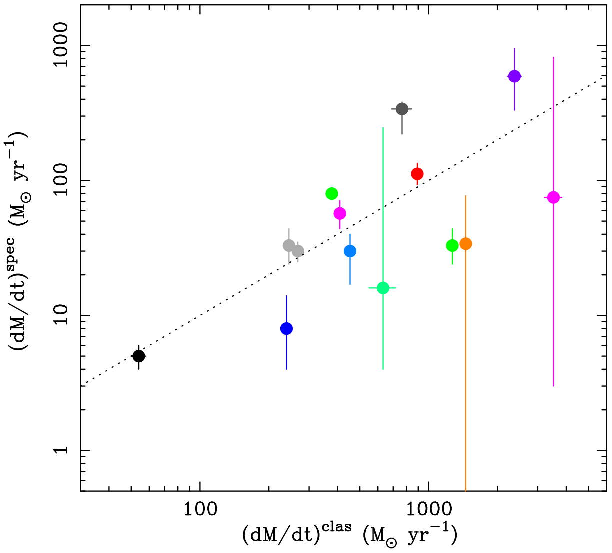

Figure 4. The total spectral mass deposition rate within the cooling radius plotted against the classic mass deposition rate. The dashed line indicates where the spectrally-determined mass deposition rate would be one-tenth of the classic mass deposition rate.

7 TURBULENT HEAT TRANSPORT

Cho et al. (2003) suggest that turbulent heat transport by mixing may produce conductivities at least as high as those advocated by Narayan & Medvedev (2001). They derive a coefficient of turbulent diffusion $\kappa_{\rm diff} = C_{\rm dyn} L V_{\rm L}$, where $V_{\rm L}$ is the amplitude of the r.m.s. turbulent velocity, L is the scale length of the turbulent motions and $C_{\rm dyn}$ is a constant of the order unity. The turbulent conductivity is then given by $\kappa_{\rm turb} = n_{\rm e} k \kappa_{\rm diff}$.

Assuming $V_{\rm L} = \alpha c_{\rm s}$, where $c_{\rm s}$ is the gas sound speed, and $L = \beta r$, then

$$\kappa_{\rm turb} = \alpha\beta n_{\rm e} k^{\frac{3}{2}} r \left(\frac{\gamma}{\mu m_{\rm H}}\right)^{\frac{1}{2}} T^{\frac{1}{2}} \qquad (15)$$

where $\alpha, \beta \leq 1$.

Since the dependence of electron number density on temperature varies from cluster to cluster, we find a general expression for $\kappa_{\rm turb}$ by calculating $n_{\rm e}$ as a function of temperature at a fixed cooling time.

For $T \gtrsim 3 \times 10^7$ K, thermal bremsstrahlung is the main emission mechanism and $\epsilon \approx 3.0 \times 10^{-27} n_{\rm h}^2 T^{\frac{1}{2}}$ erg cm^{-3} s^{-1}. For $T \lesssim 3 \times 10^7$ line cooling becomes important and $\epsilon \approx 6.2 \times 10^{-19} n_{\rm h}^2 T^{-\frac{3}{5}}$ erg cm^{-3} s^{-1} (McKee & Cowie 1977). Substituting ϵ into Equation 5 we can re-write $t^{\rm cool}$ in terms of the temperature and electron number density in the two temperature regimes

$$t_j^{\rm cool} \approx 2.0 \times 10^{10} \left(\frac{n_{\rm e}}{10^{-3}\ {\rm cm}^{-3}}\right)^{-1} \left(\frac{T}{10^7\ {\rm K}}\right)^{\frac{1}{2}} {\rm yr}, \qquad (16)$$

$$T \gtrsim 3 \times 10^7\ {\rm K}$$

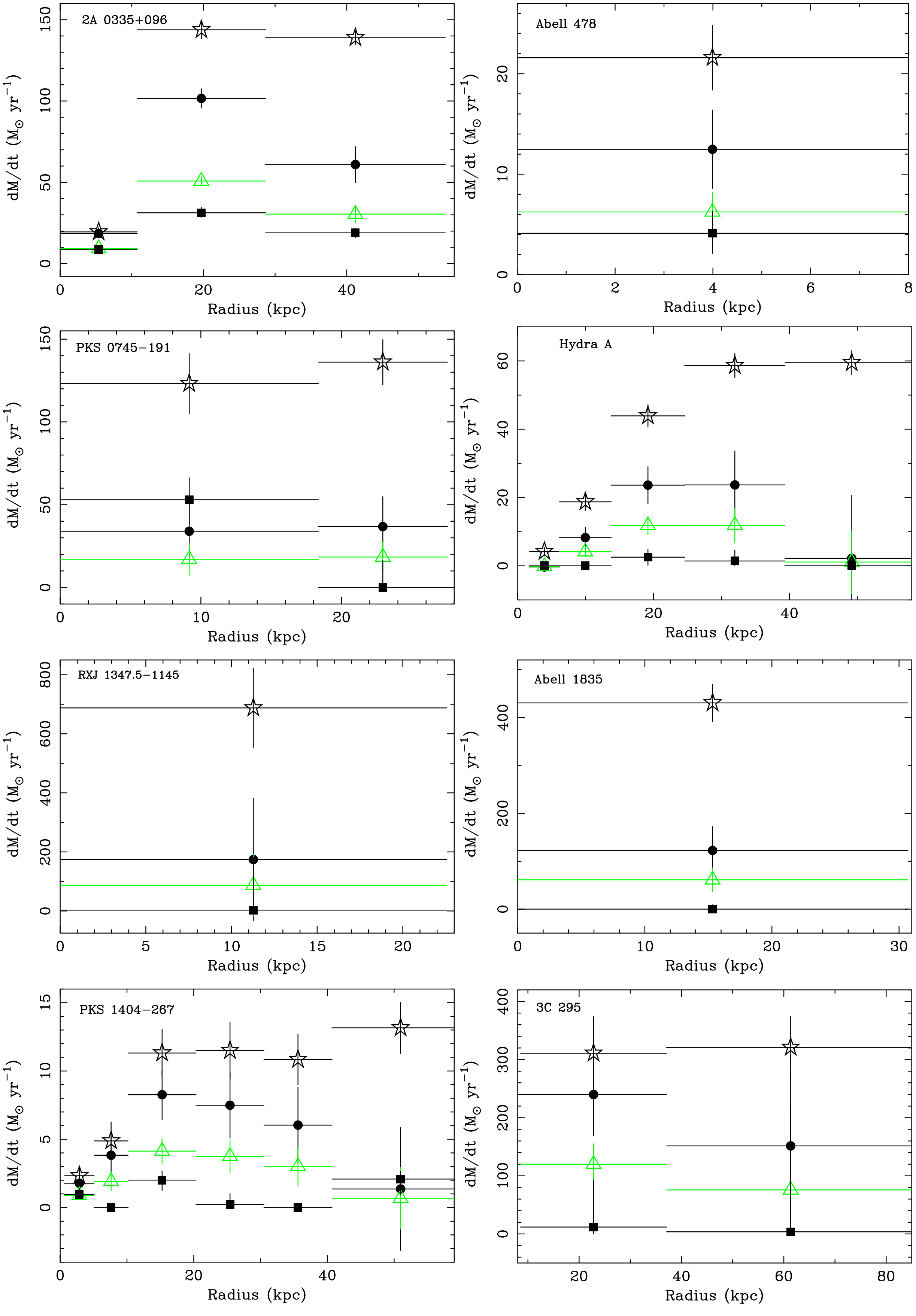
2A 0335+096
Abell 478
PKS 0745−191
Hydra A
RXJ 1347.5−1145
Abell 1835
PKS 1404−267
3C 295
dM/dt (M⊙ yr⁻¹)
Radius (kpc)
0
50
100
150
0
10
20
0
2
4
6
8
0
20
40
60
0
200
400
600
800
0
5
10
15
20
30
80

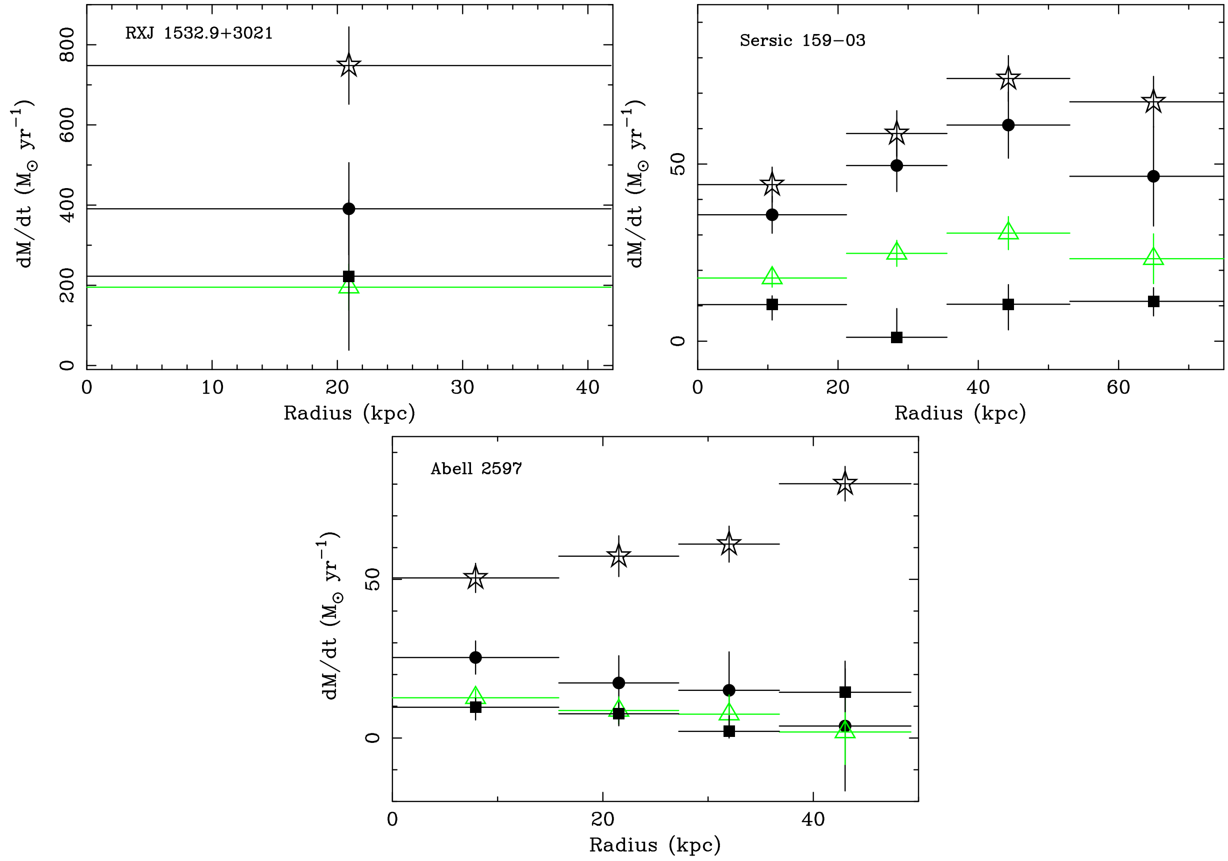

Figure 2. Classic mass deposition rates (open stars), mass deposition rates assuming conduction at the Spitzer rate (filled circles) and spectral mass deposition rates (filled squares) for clusters where $\kappa^{\rm eff} > \kappa_{\rm S}$ (with the exception of M87). The grey open triangles are the cooling rates calculated assuming conduction at the Spitzer rate, reduced by a factor of 2 to take into account the gravitational contribution to the luminosity.

and

$$t_j^{\rm cool} \approx 0.5 \times 10^{10} \left(\frac{n_{\rm e}}{10^{-3}\ {\rm cm}^{-3}}\right)^{-1} \left(\frac{T}{10^7\ {\rm K}}\right)^{\frac{8}{5}} {\rm yr}, \qquad (17)$$

$$T \lesssim 3 \times 10^7\ {\rm K}.$$

Substituting Equations 16 and 17 into Equation 15 we find the following expressions for the turbulent conductivity at a fixed cooling time within each cluster

$$\kappa_{\rm turb} \approx 8 \times 10^{12} \left(\frac{T}{10^7\ {\rm K}}\right) {\rm erg\,s^{-1}\,cm^{-1}\,K^{-1}}, \qquad (18)$$

$$T \gtrsim 3 \times 10^7\ {\rm K}$$

and

$$\kappa_{\rm turb} \approx 2 \times 10^{12} \left(\frac{T}{10^7\ {\rm K}}\right)^{2.1} {\rm erg\,s^{-1}\,cm^{-1}\,K^{-1}}, \qquad (19)$$

$$T \lesssim 3 \times 10^7\ {\rm K}$$

for $\alpha\beta$=1, $\gamma = \frac{5}{3}$, $t^{\rm cool}$= 1Gyr and L = 20 kpc. (In the lower plot in Fig. 1 we see that $L \approx 20$ kpc at $t^{\rm cool}$=1Gyr for the clusters in the sample). We plot this curve on the effective conductivity plot in Fig. 1. Turbulent heat transport may be important, depending on the actual values of α and β.

We also compute a $\kappa_{\rm turb}$ profile for each cluster individually (shown in Fig. 8) using Equation 15. The $\kappa_{\rm turb}$ and $\kappa^{\rm eff}$ profiles are strikingly similar if $\alpha\beta \sim \frac{1}{2} - \frac{1}{10}$. This may be explained by the scaling involved. We have that

$$\frac{\kappa^{\rm eff}}{\kappa_{\rm turb}} \propto \frac{n_{\rm e}}{{\rm dT/dr}} = \frac{n_{\rm e} r}{T} \qquad (20)$$

for power-law temperature profiles and bremsstrahlung emission. Typically $n_{\rm e} r \sim$ constant and T varies at most by a factor of ~ 3. The similarity could therefore be a coincidence. More interestingly, the scaling (i.e. the temperature and density profiles observed) could result from turbulence *being* the heat transport process operating in cluster cores.

One problem with the last possibility is that the quasi-linear optical filaments seen in the Perseus cluster (Conselice et al. 2001) argue in that case against the gas being strongly turbulent (Fabian et al. 2003c). A mild circulation pattern with eddies of a few kpc driven by buoyant radio bubbles and oscillatory motion of the central galaxy may however be consistent.

8 RADIO AND OPTICAL DATA

If the intracluster gas is heated by the central radio source, then we would expect to see some degree of correlation between the heating rate required to prevent cooling and the radio luminosity of the central source. In Table 5 we show the radio luminosities measured at 20 cm (1.4 GHz), obtained from the NVSS survey (Condon et al. 1998). In each case the radio sources detected within 15 arcsec of the X-ray centre (see Table 1) are tabulated. We plot the rate of

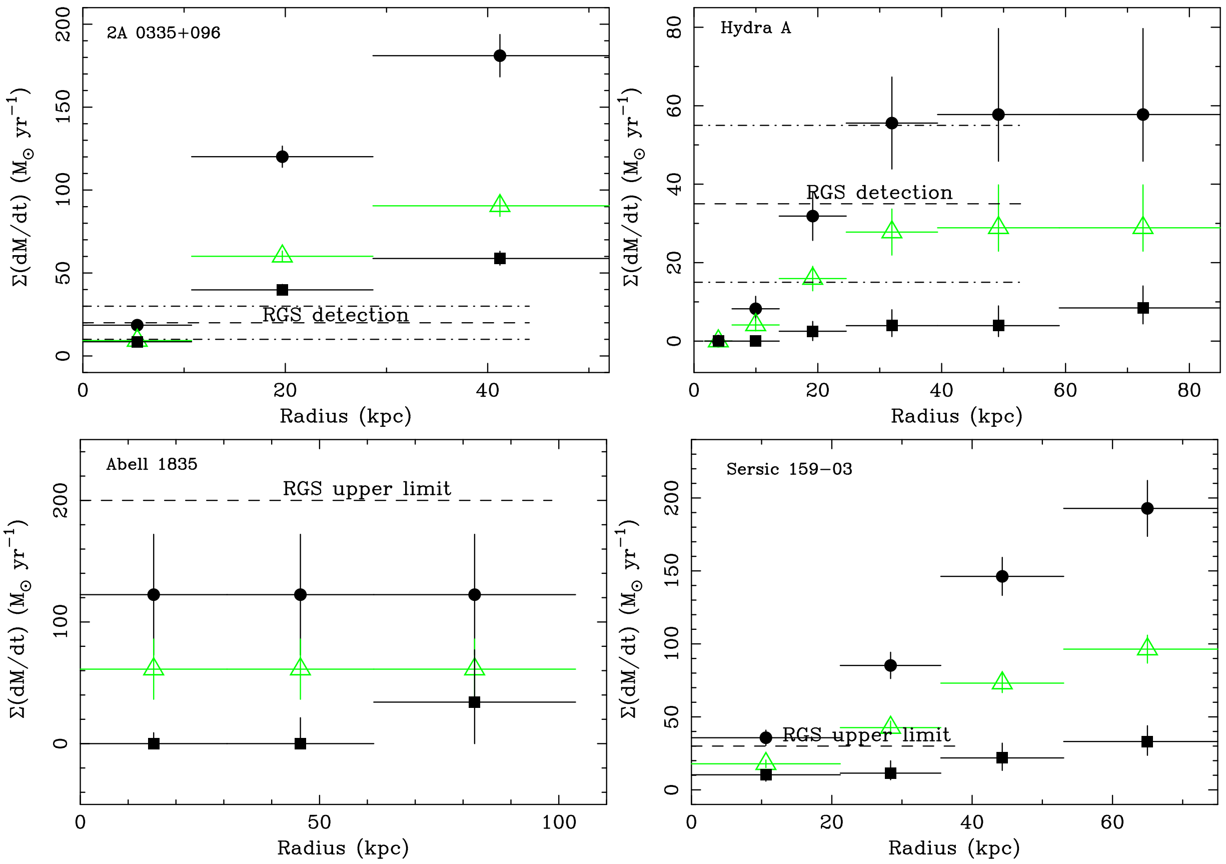

Figure 3. As for Fig. 2, but with the mass deposition rates summed out to the radius shown. The upper limits and detections of cool gas from RGS data (Peterson et al. 2002) are shown by dashed lines (with the error bars shown by the dash-dot lines). The minimum $\dot{M}$ value from the three temperature bands used by Peterson et al. (2002) is plotted in each case.

energy loss from the cluster within the cooling radius against the total 1.4 GHz radio luminosity in Fig. 5.

We see that there is no obvious correlation between the radio power observed and the radio power required to prevent cooling in these clusters. Although the radio luminosity is not directly related to the mechanical power of the radio lobes, it is unlikely that the same PdV work can be done on clusters with similar X-ray luminosities when their radio source luminosities vary by over 5 orders of magnitude.

Observations in the UV, optical and infrared suggest that a small cooling flow may be required to fuel the observed star formation rates, emission line nebulosities and molecular gas masses (Donahue 2000; Edge 2001; Edge et al. 2002) in the centres of cooling flow galaxy clusters. In Table 5 we indicate whether or not optical emission lines have been observed in the object (Crawford & Fabian 1992; Crawford et al. 1999; Peres et al. 1998).

It is interesting that there is no evidence for optical emission lines in Abell 2029 (Johnstone et al. 1987; McNamara & O'Connell 1989), given that conduction at $\kappa \sim (0.3\text{–}0.4)\ \kappa_{\rm S}$, the range in plasma conductivity advocated by Narayan & Medvedev 2001, can prevent cooling from taking place right into the inner few kpc of this object.

We also note that molecular gas is generally found only within the central ~ 20 kpc of clusters (Donahue & Voit 2003); indicating that if we are indeed detecting the cool sink produced by a reduced cooling flow, then any heat process operating in these objects fails to stop cooling only in the innermost region. We find that, in general, the effective conductivity profiles rise above the Spitzer curve towards the centres of the clusters.

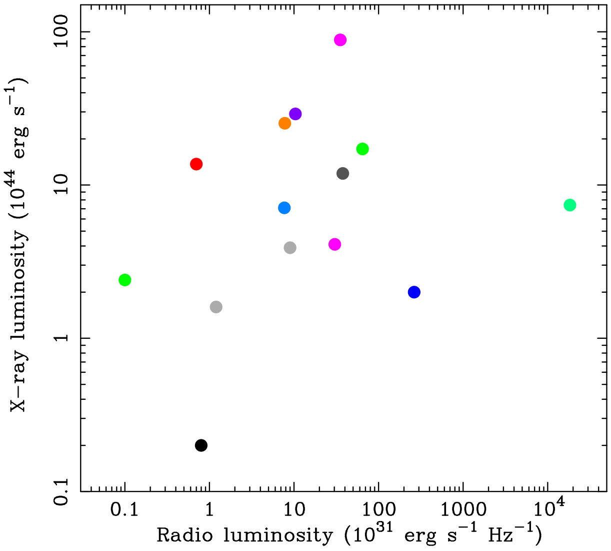

Figure 5. The total X-ray luminosity emitted from within the cooling radius of each cluster against the total 1.4 GHz radio power within 15 arsec of the cluster X-ray centre.

Cluster	Position (J2000)		Flux	Total Radio Luminosity	X-ray Luminosity	Optical lines
	RA	Dec	(mJy)	(10^{31} erg s^{-1} Hz^{-1})	(10^{44} erg s^{-1})	
2A0335+096	(03 38 40.62)	(+09 58 12.2)	36.7	0.1	2.3	YES
	(03 38 40.06)	(+09 58 11.0)	1.8			
A478	(04 13 25.18)	(+10 27 54.1)	36.9	0.7	13.6	YES
	(04 13 20.04)	(+10 27 50.7)	1.5			
PKS 0745-191	(07 47 31.35)	(07 47 30.0)	2372.0	64.7	17.2	YES
	(07 47 30.03)	(-19 17 30.6)	83.7			
Hydra A	(09 18 05.78)	(-12 05 41.3)	40849.9	263.9	2.0	YES
	(09 18 00.03)	(-12 05 40.6)	1278.8			
M87	(12 30 49.46)	(+12 23 21.6)	138487.0	5.7	–	YES
	(12 30 00.03)	(+12 23 20.3)	4858.7			
RXJ 1347.5-1145	(13 47 30.67)	(-11 45 08.6)	45.9	35.3	89.0	–
	(13 47 30.04)	(-11 45 00.7)	1.5			
A1795	(13 48 52.43)	(+26 35 33.6)	924.5	9.0	3.7	YES
	(13 48 50.03)	(+26 35 30.6)	27.7			
A1835	(14 01 02.05)	(+02 52 41.0)	39.3	7.8	26.0	YES
	(14 01 00.04)	(+02 52 40.7)	1.6			
PKS 1404-267	(14 07 29.83)	(-27 01 04.2)	645.5	0.8	0.17	–
	(14 07 20.03)	(-27 01 00.6)	22.8			
3C295	(14 11 20.63)	(+52 12 09.0)	22720.1	1.83×10^4	7.2	–
	(14 11 20.05)	(+52 12 00.6)	681.6			
A2029	(15 10 55.87)	(+05 44 39.3)	527.8	7.7	6.9	NO
	(15 10 50.03)	(+05 44 30.6)	18.2			
RXJ 1532.9+3021	(15 32 53.77)	(+30 20 59.8)	22.8	10.4	27.5	YES
	(15 32 50.06)	(+30 20 50.8)	0.8			
Cygnus A	(19 59 28.1)	(40 44 0.5.00)	5.7×10^5	4.2×10^3	–	YES
A2390	(21 53 36.81)	(+17 41 44.8)	235.3	37.8	11.4	YES
	(21 53 30.06)	(+17 41 40.6)	8.3			
Sersic 159-03	(23 13 58.60)	(-42 43 38.0)	156.7	1.2	1.9	YES
A2597	(23 25 19.82)	(-12 07 28.6)	1874.6	30.4	4.0	YES
	(23 25 10.03)	(-12 07 20.6)	56.2			

Table 5. 1.4 GHz radio fluxes from within 15 arcsec of the X-ray peak (from the NVSS survey; Condon et al. 1998), radio luminosities calculated from the radio fluxes and X-ray luminosity from within the cooling radius. The 1.4 GHz radio fluxes for Cygnus A and Sersic 159-03 were found using 4.85 GHz data from the Green Bank and PMN (Wright et al. 1994) surveys respectively, assuming $I_\nu \propto \nu^{-\alpha}$, with α=0.8. In the last column we indicate the presence, absence or lack of information on optical emission lines in the cluster (Crawford & Fabian 1992; Crawford et al. 1999; Peres et al. 1998).

9 DISCUSSION

We have carried out spatially-resolved, deprojected analyses of the cooling flow regions in a sample of galaxy clusters and find effective conductivity profiles which lie both above and below the Spitzer curve. If the plasma conductivity in galaxy clusters is close to the unhindered Spitzer value, then conduction will play a important role in reducing cooling flows.

For clusters with effective conductivity values above the Spitzer curve, we calculated the rate at which gas must cool out of the ambient plasma, assuming unhindered conduction, and found spectral mass deposition rates at least a factor of two lower than is required for energy balance in five objects.

The possibility that the plasma conductivity is as high as 0.1–1.0 $\kappa_{\rm S}$ continues to be debated in the literature, both from an observational viewpoint (Ettori & Fabian; Vikhlinin et al. 2001; Markevitch et al. 2003; Nath 2003) and theoretically (Chandran & Cowley 1998; Narayan & Medvedev 2001; Chandran & Maron 2003). We also point out that a certain amount of fine-tuning is required for the conduction model to be successful. For an energy balance between conduction and cooling to exist in each object, the suppression factor must vary from cluster to cluster. However, it is not unreasonable to expect there to be some variation in the suppression of conduction in different objects; in particular since rotation measures show that the length over which fields are ordered varies between clusters (Taylor et al. 2002). Also, mass inflow itself may pull the field lines radially, increasing the conductivity (Bregman & David 1988; Fabian et al. 2002b).

Since the model requires some finite $\dot{M}$ in most clusters, we must consider whether or not it is physically plausible for an inhomogeneous cooling flow to exist in a conducting medium. If the gas which cools out of the flow 'pulls' magnetic field lines around it as it condenses then the cool blobs may be magnetically isolated from the surrounding hotter, conducting medium. We note that a certain amount of cool gas may need be deposited in the centres of galaxy clusters in order to account for the enhanced star formation rates (Crawford et al. 1999) and molecular gas masses detected (Edge 2001; Edge et al. 2002).

In this paper we concentrate on the energetic feasibility of balancing bremsstrahlung emission with conductive heat transfer. For the conduction model to be successful, this balance must be stable; or at least quasi-stable over the timescales considered. The conduction scenario may be a self-regulating process. Radiative cooling occurs isobarically at each radius and so a perturbation causing the temperature to drop leads to an increase in the cooling rate. We might then expect the gas to cool dramatically since conductivity decreases with temperature. However, the decline in temperature leads to an increase in the temperature gradient, which is beneficial for conductive heat transfer. The situation is complex and time-dependent simulations are needed to understand how the intracluster gas may evolve. Past work has shown that steady state solutions to the energy equation are unable to reproduce the large temperature gradients observed (Bregman & David 1988; Bertschinger & Meiksin 1986; Meiksin 1988). Zakamska & Narayan (2002), on the other hand, argue that the balance is stable with the observed temperature and density profiles. Kim & Narayan (2003) suggest that thermal instabilities are unimportant on timescales $\sim$ 2–5 Gyr.

If there is some heating process preventing cooling flows from developing then it must be distributed. We see from Fig. 6 (left plot) that the heat which must be transferred per kpc to shells at increasing radii is approximately constant between 20 and 100 kpc, with a rise in the innermost region. If the cluster is heated by the central AGN then the $P\mathrm{d}V$ work done in blowing bubbles through the intracluster medium must lead to the widespread deposition of energy. How this heat is transported is unclear (viscous dissipation of the sound waves produced by the bubbles is a possibility; Fabian et al. 2003b). It has been suggested that conduction and AGN heating work together in galaxy clusters (Brighenti & Matthews 2003, Ruszkowski & Begelman 2002), and, in particular, that conduction prevents cooling in the outer regions, with AGN heating dominating in the inner regions (Kim & Narayan 2003). Since we find κ^{eff} decreases with radius in most clusters it would be worth pursuing this scenario. We plot the heating rate required per kpc with conduction at $\kappa = \kappa_{\mathrm{S}}/3$ (right plot in Fig. 6). The required heating is little changed for the cooler clusters in our sample.

10 SUMMARY

Recent *XMM-Newton* observations using the RGS have shown that although cooling may have occurred in the past, it is likely that some heating mechanism is preventing net heat loss at the observed epochs ($z = 0.0 - 0.5$). We have shown that, in general, conduction at close to the Spitzer rate is able to completely offset cooling in the hotter parts of clusters ($T \gtrsim 5$ keV). But in the inner, cooler parts of hot clusters and most of cool clusters conduction is insufficient. The observed spectral mass deposition rates found here are less than the amounts expected from the radiative cooling rate and some additional heating and/or absorption of the cooling gas is therefore required.

It has been suggested that turbulent heat diffusion can provide a high effective heat conductivity (Cho et al. 2003). We have shown that this process may supply adequate heat to balance radiative cooling in the observed clusters. In detail, it provides remarkably similar profiles to those required.

11 ACKNOWLEDGEMENTS

We thank Roderick Johnstone for help with the analysis of PKS 1404-267 and the use of his program for evaluating the cooling function. We are also grateful to Robert Schmidt and Jeremy Sanders for the use of their scripts in the Monte Carlo simulations and cooling flow models, respectively. We thank Steve Allen and Martin Laming for helpful discussions. ACF and LMV acknowledge support from The Royal Society and PPARC, respectively.

REFERENCES

Allen S. W., Ettori S., Fabian A. C., 2001a, MNRAS, 324, 877
Allen S. W., Taylor G. B., Nulsen P. E. J., Johnstone R. M. J., David L. P., Ettori S., Fabian A. C., Forman W., Jones C., McNamara B., 2001b, MNRAS, 324, 842
Allen S. W., Schmidt R. W., Fabian A. C., 2002, MNRAS, 335, 256
Anders E., Grevesse N., 1989, Geochimica et Cosmochimica Acta 53, 197
Arnaud K. A., 1996, in Astronomical Data Analysis Software and Systems V, eds. Jacoby G., Barns J., ASP Conf. Ser., 101, 17
Arnaud M., Evrard A. E., 1999, MNRAS, 305, 631
Balusinska-Church M., McCammon D., 1992, ApJ, 400, 699
Barnes D. G., Nulsen P. E. J., 2003, submitted MNRAS , astro-ph/0304065
Bertschinger E., Meiksin A., 1986, ApJ, 306, L1
Böhringer H. et al., 2001, A&A, 365, L181
Bregman J. N., David L. P., 1988, ApJ, 326, 639
Brighenti F., Matthews W. G., 2003, ApJ, 587, 580
Brüggen M., Kaiser C. R., 2001, MNRAS, 325, 676
Carilli C. L., Taylor G. B., 2002, ARA&A, 40, 319
Chandran B. D. G., Cowley S. C., 1998, Phys. Rev. Lett., 80, 3077
Chandran B. D. G., Maron J. L., 2003, submitted ApJ, astro-ph/0303214
Cho J., Lazarian A., Honein A., Knaepen B., Kassinos S., Moin P., 2003, submitted ApJ, astro-ph/0302503
Churazov E., Brüggen M., Kaiser C. R., Böhringer H., Forman W., 2001, ApJ, 554, 261
Condon J. J., Cotton W. D., Greisen E. W., Yin Q. F., Perley R. A., Taylor G. B., Broderick J. J., 1998, AJ, 115,1693
Conselice C. J., Gallagher J. S., Wyse R. F. G., 2001, AJ, 122, 2281
Cowie L. L., McKee C. F., 1977, ApJ, 211, 135
Crawford C. S., Fabian A. C., 1992, MNRAS, 259, 265
Crawford C. S., Allen S. W., Ebeling H., Edge A. C., Fabian A. C., 1999, MNRAS, 306, 857
David L. P., Slyz A., Jones C., Forman W., Vrtilek S. D., Arnaud K. A., 1993, ApJ, 412, 479
David L. P., Nulsen P. E. J., McNamara B. R., Forman W., Jones C., Ponman T., Robertson B., Wise M., 2001, 557, 546
De Grandi S., Molendi S., 1999, A&A, 351, L45
Di Matteo T., Allen S. W., Fabian A. C., Wilson A. S., Young A. J., 2003. ApJ, 582, 133
Dickey J. M., Lockman F. J., 1990, ARA&A, 28, 215
Donahue M., Mack J., Voit M., Sparks W., Elston R., Maloney P. R., 2000, ApJ, 545, 670
Donahue M., Voit M., 2003, Carnegie Obs. Astrophys. Ser., Vol. 3, astro-ph/0308006
Edge A. C., 2001, MNRAS, 328, 762
Edge A. C., Wilman R. J., Johnstone R. M., Crawford C. S., Fabian A. C., Allen S. W., 2002, MNRAS, 337, 49
Ettori S., Fabian A. C., 2000, MNRAS, 317 L57
Ettori S., Allen S. W., Fabian A. C., 2001, MNRAS, 322, 187
Ettori S., Fabian A. C., Allen S. W., Johnstone R. M., 2002, MNRAS, 331, 635
Fabian A. C. et al., 1985, MNRAS, 216, 923
Fabian A. C., 1994, ARAA, 32, 227
Fabian A. C., Mushotzky R. F., Nulsen P. E. J., Peterson J. R., 2001, MNRAS, 321, L20
Fabian A. C., Allen S. W., Crawford C. S., Johnstone R. M., Morris R. G., Sanders J. S., Schmidt R. W., 2002a, MNRAS, 332, L50
Fabian A. C., Voigt L. M., Morris R. G., MNRAS, 2002b, 335, L71
Fabian A. C., 2003a, accepted MNRAS, in press
Fabian A. C., Sanders J. S., Allen S. W., Crawford C. S., Iwasawa K., Johnstone R. M., Schmidt R. W., Taylor G. B., 2003b, MNRAS accepted, astro-ph/0306036
Fabian A. C., Sanders J. S., Crawford C. S., Conselice C. J., Gallagher III J. S., Wyse R. F. G., 2003c, MNRAS accepted, astro-ph/0306039
Gruzinov A., 2002, astro-ph/0203031
Hicks A. K., Wise M. W., Houck J. C., Canizares C. R., 2002, ApJ, 580, 763
Johnstone R. M., Fabian A. C., Nulsen P. E. J., 1987, MNRAS, 224, 75

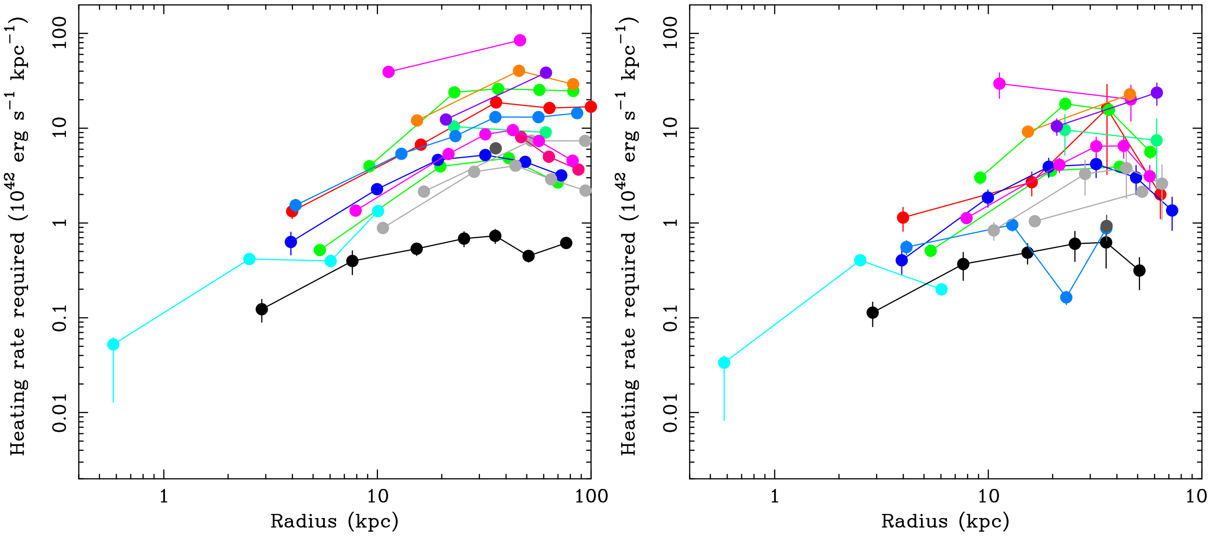

Figure 6. Heating rate required per kpc at increasing radii within the central 100 kpc, with $\kappa = 0$ (left) and $\kappa = \kappa_{\rm S}/3$ (right). Cygnus A does not appear in the plot on the right since conduction below one-third the Spitzer rate offsets cooling completely in this object.

Johnstone R. M., Fabian A. C., Edge A. C., Thomas P. A., 1992, MNRAS, 255, 431

Johnstone R. M., Fabian A. C., Taylor G. B., 1998, MNRAS, 298, 854

Johnstone R. M., Allen S.W., Fabian A. C., Sanders J.S., 2002, MNRAS, 336, 299

Kaastra J. S., Ferrigno C., Tamura T., Paerels F. B. S., Peterson J. R., Mittaz J. P. D., 2001, A&A, 365, L99

Kim W.,, Narayan R., 2003, accepted ApJ, astro-ph/0303097

Lewis A. D., Stocke J. T., Buote D. A., 2002, ApJ, 573, L13

Liedahl D. A., Osterheld A. L., Goldstein W. H., 1995, ApJ, 438, L115

Loeb A., 2002, New Astronomy, 7, 279

Markevitch M., 1998, ApJ, 504, 27

Markevitch M. et al., 2003, ApJ, 586, L19

Maron J. L., Chandran B. D. G., Blackman E. G., 2003, submitted Phys. Rev. Lett., astro-ph/0303217

Matsushita K., Belsole E., Finoguenov A., Böhringer H., 2002, A&A, 386, 77

Mazzotta P., Edge A., Markevitch M., 2003, submitted ApJ, astro-ph/0303314

McKee C. F., Cowie L. L., 1977, ApJ, 215, 213

McNamara B. R., O'Connell R. W., 1989, ApJ, 98, 6

McNamara B. R., Wise M., Nulsen P. E. J., David L. P., Sarazin C. L., Bautz M., Markevitch M., Vikhlinin A., Forman W. R., Jones C., Harris D. E., 2000, ApJ, 534, L135

McNamara B. R. et al., 2001, ApJ, 562, L149

Medvedev M. V., Melott A. L., Miller C., Horner D., 2003, astro-ph/0303310

Mewe R., Gronenschild E. H. B. M., van den Oord G. H. J., 1985, A&AS, 62, 197

Molendi S., 2002, ApJ, 580, 815

Molendi S., Pizzolato F., 2001, ApJ, 560, 194

Morris R. G., Fabian A. C., 2003, MNRAS, 338, 824

Narayan R., Medvedev M. V., 2001, ApJ, 562, L129

Peres C. B., Fabian A. C., Edge A. C., Allen S. W., Johnstone R. M., White D. A., 1998, MNRAS, 298, 416

Nath B. B., 2003, MNRAS, 340, L1

Peterson J. R. et al., 2001, A&A, 365, L104

Peterson J. R., Kahn S. M., Paerels F. B. S., Kaastra J. S., Tamura T., Bleeker J. A. M., Ferrigno C., 2002, ApJ, 590, 207

Rechester A. B., Rosenbluth M. N., 1978, Phys. Rev. Lett., 40, 33

Ruszkowski M.,, Begelman M. C., 2002, ApJ, 581, 223

Salem C., Hubert D., Lacombe C., Bale S. D., Mangeney A., Larson D. E., Lin R. P., 2003, ApJ, 585, 1147

Schmidt R. W., Allen S. W., Fabian A. C., 2001, MNRAS, 327, 1057

Smith D. A., Wilson A. S., Arnaud K. A., Terashima Y., Young A. J., 2002, ApJ, 565, 195

Spitzer L., 1962, Physics of Fully Ionized Gases, New York: Wiley-Interscience

Sun M., Jones C., Murray S. S., Allen S. W., Fabian A. C., Edge A. C., 2003, ApJ, 587, 619

Takizawa M., Sarazin C. L., Blanton E. L., Taylor G. B., 2003, accepted ApJ, astro-ph/0306157

Tamura T., Kaastra J. S., Peterson J. R., Paerels F. B. S., Mittaz J. P. D., Trudolyubov S. P., Stewart G., Fabian A. C. F., Mushotzky R. F., Lumb D. H., Ikebe Y., 2001, A&A, 365, L87

Taylor G. B., Allen S. W., Fabian A. C., 2002. MNRAS, 334, 769

Tucker W.H., Rosner R., 1983, ApJ, 267, 547

Vikhlinin A., Markevitch M., Forman W., Jones C., 2001, ApJ, 555, L87

Voigt L. M., Schmidt R. W., Fabian A. C., Allen S. W., Johnstone R. M., MNRAS, 335, L7

Wright A. E., Griffith M. R., Burke B. F., Ekers R. D., 1994, ApJ, 91, 111

Young A. J., Wilson A. S., Mundell C. G., 2002, ApJ, 579, 560

Zakamska N. L., Narayan R., 2003, ApJ, 582, 162

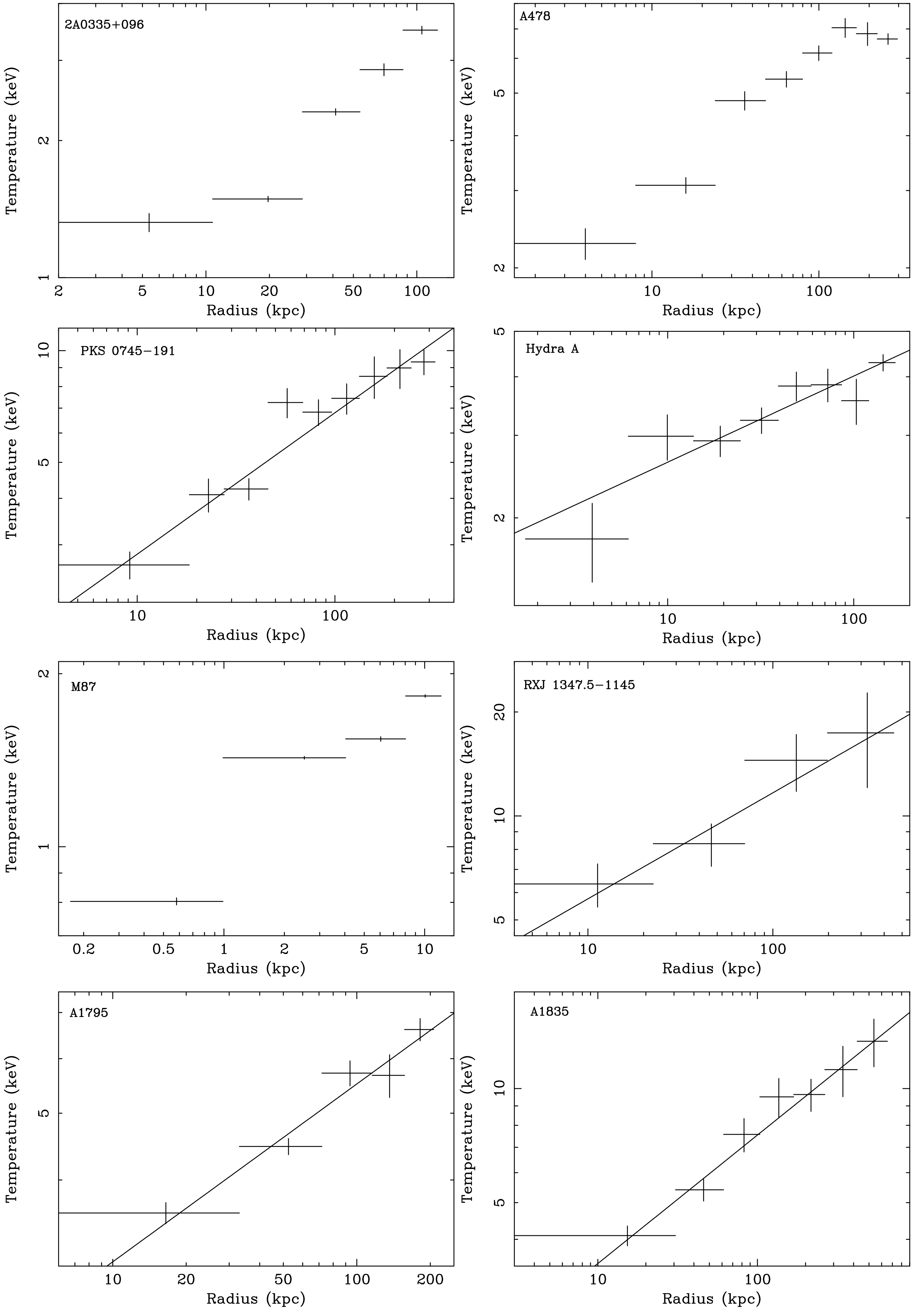
2A0335+096
Temperature (keV)
1
2
Radius (kpc)
2
5
10
20
50
100
A478
Temperature (keV)
2
5
Radius (kpc)
10
100
PKS 0745−191
Temperature (keV)
5
10
Radius (kpc)
10
100
Hydra A
Temperature (keV)
2
5
Radius (kpc)
10
100
M87
Temperature (keV)
1
2
Radius (kpc)
0.2
0.5
1
2
5
10
RXJ 1347.5−1145
Temperature (keV)
5
10
20
Radius (kpc)
10
100
A1795
Temperature (keV)
5
Radius (kpc)
10
20
50
100
200
A1835
Temperature (keV)
5
10
Radius (kpc)
10
100

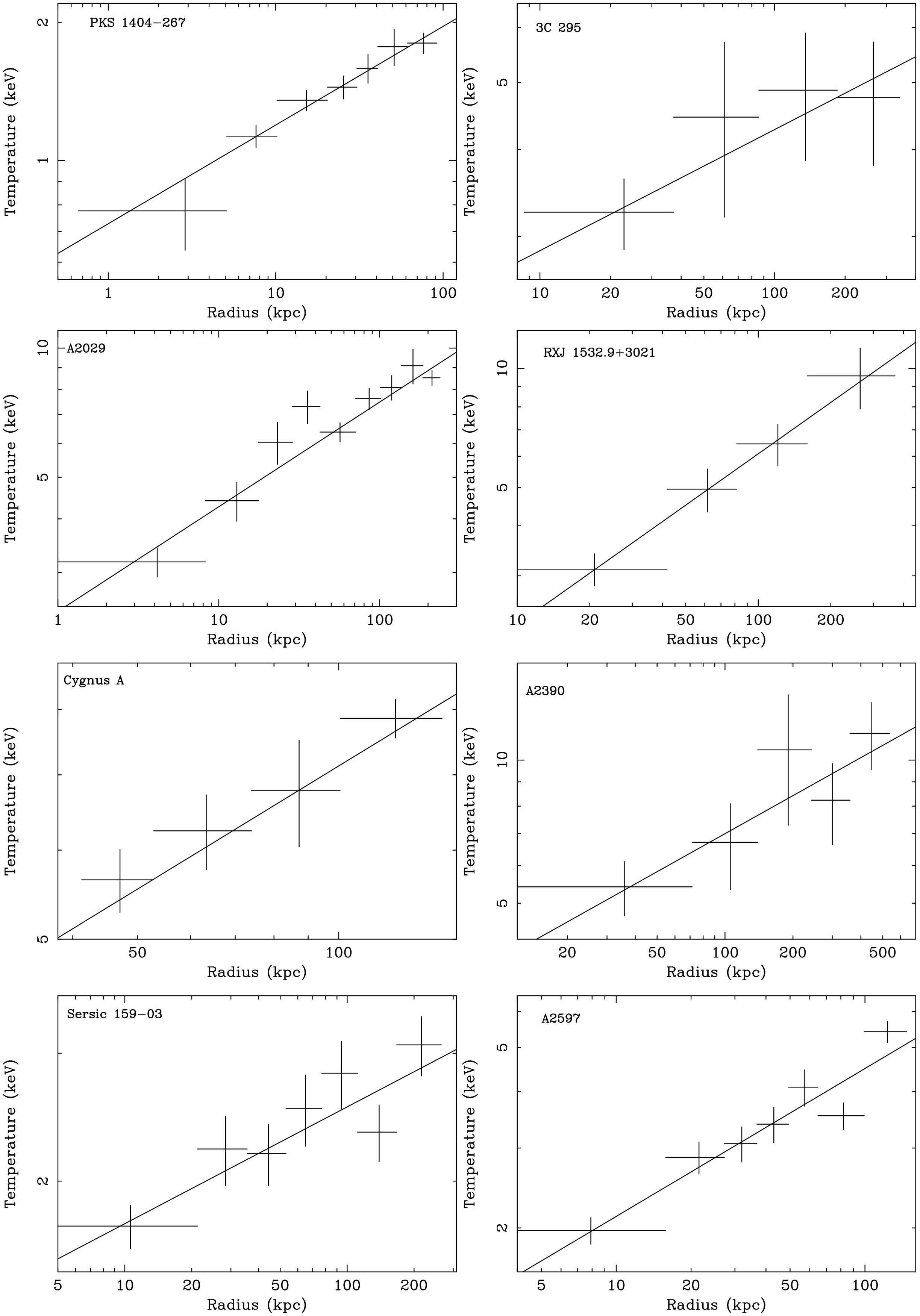

Figure 7. Deprojected temperature profiles obtained using the model PROJCT*PHABS(MEKAL) in XSPEC . The best-fitting power law to the data is shown for clusters with over-lapping error bars.

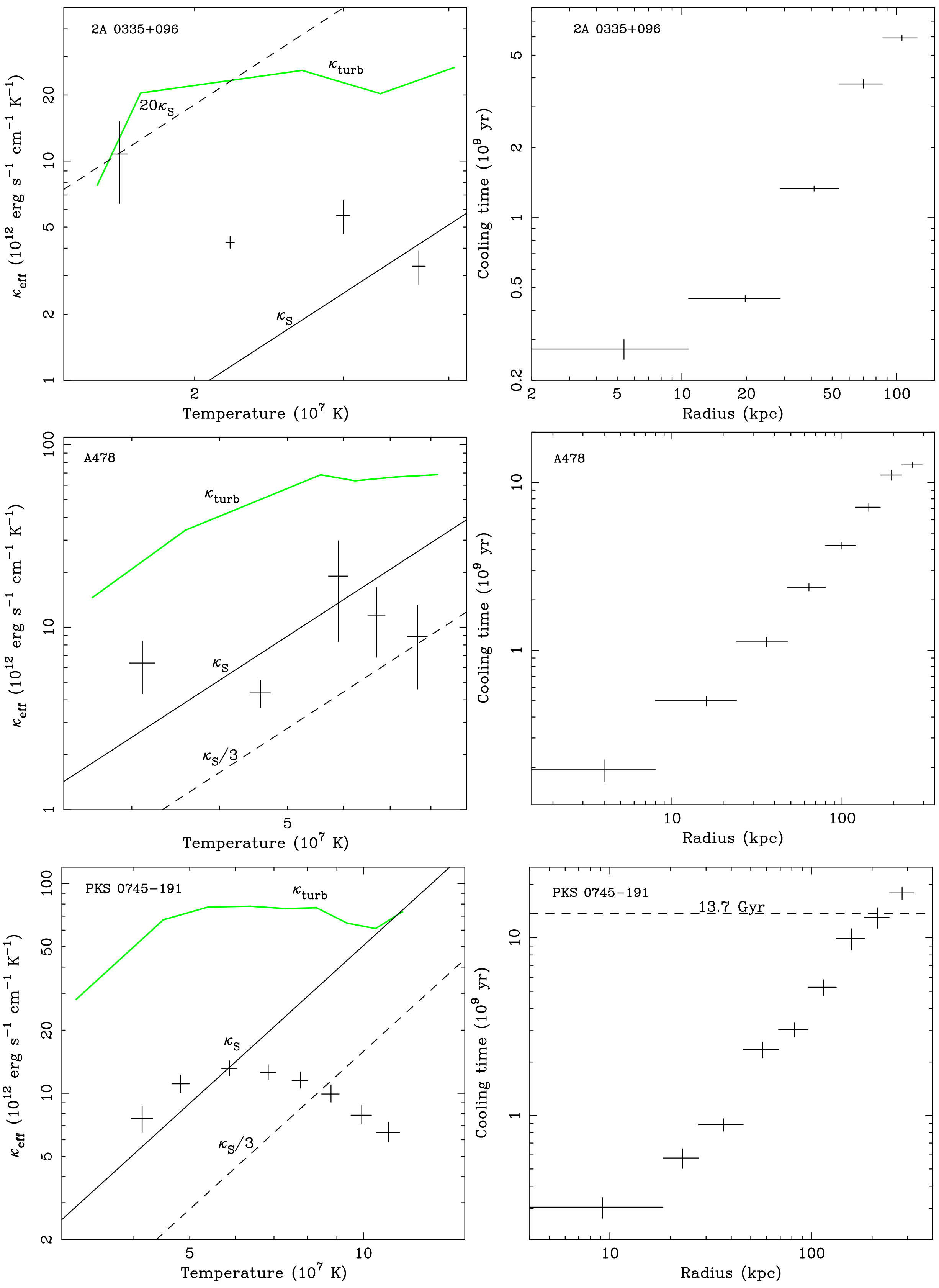
2A 0335+096
$\kappa_{\rm turb}$
$20\kappa_{\rm S}$
$\kappa_{\rm S}$
$\kappa_{\rm eff}$ (10^{12} erg s^{-1} cm^{-1} K^{-1})
1
2
5
10
20
Temperature (10^7 K)
2
2A 0335+096
Cooling time (10^9 yr)
0.2
0.5
1
2
5
Radius (kpc)
2
5
10
20
50
100
A478
$\kappa_{\rm turb}$
$\kappa_{\rm S}$
$\kappa_{\rm S}/3$
$\kappa_{\rm eff}$ (10^{12} erg s^{-1} cm^{-1} K^{-1})
1
10
100
Temperature (10^7 K)
5
A478
Cooling time (10^9 yr)
1
10
Radius (kpc)
10
100
PKS 0745−191
$\kappa_{\rm turb}$
$\kappa_{\rm S}$
$\kappa_{\rm S}/3$
$\kappa_{\rm eff}$ (10^{12} erg s^{-1} cm^{-1} K^{-1})
2
5
10
20
50
100
Temperature (10^7 K)
5
10
PKS 0745−191
13.7 Gyr
Cooling time (10^9 yr)
1
10
Radius (kpc)
10
100

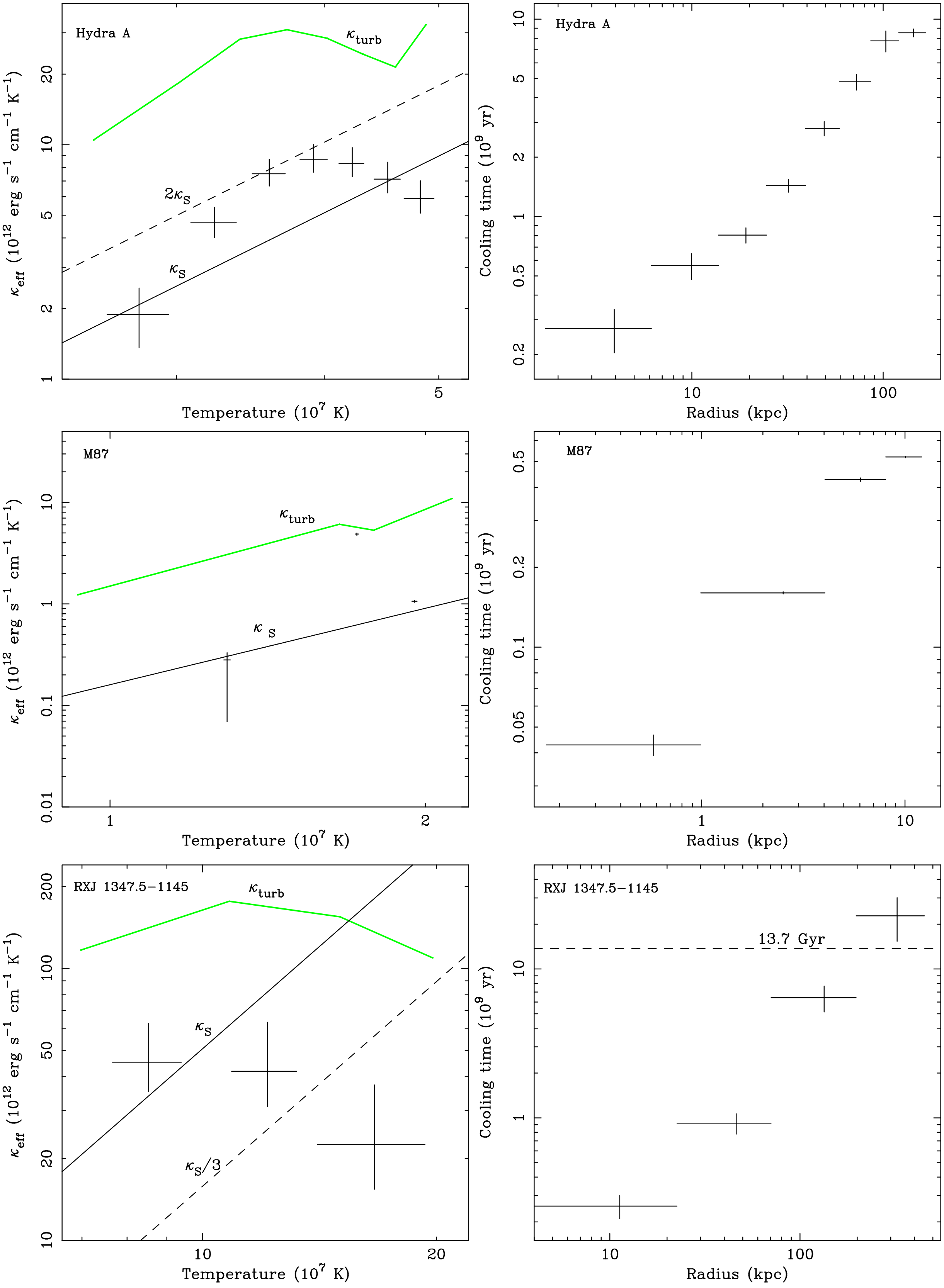
Hydra A
κturb
2κS
κS
κeff (10^12 erg s^-1 cm^-1 K^-1)
Temperature (10^7 K)
1
2
5
10
20
Hydra A
Cooling time (10^9 yr)
Radius (kpc)
0.2
0.5
1
2
5
10
100
M87
κturb
κ S
0.01
0.1
1
10
2
M87
0.05
0.1
0.2
0.5
RXJ 1347.5−1145
κturb
κS
κS/3
50
100
200
20
RXJ 1347.5−1145
13.7 Gyr

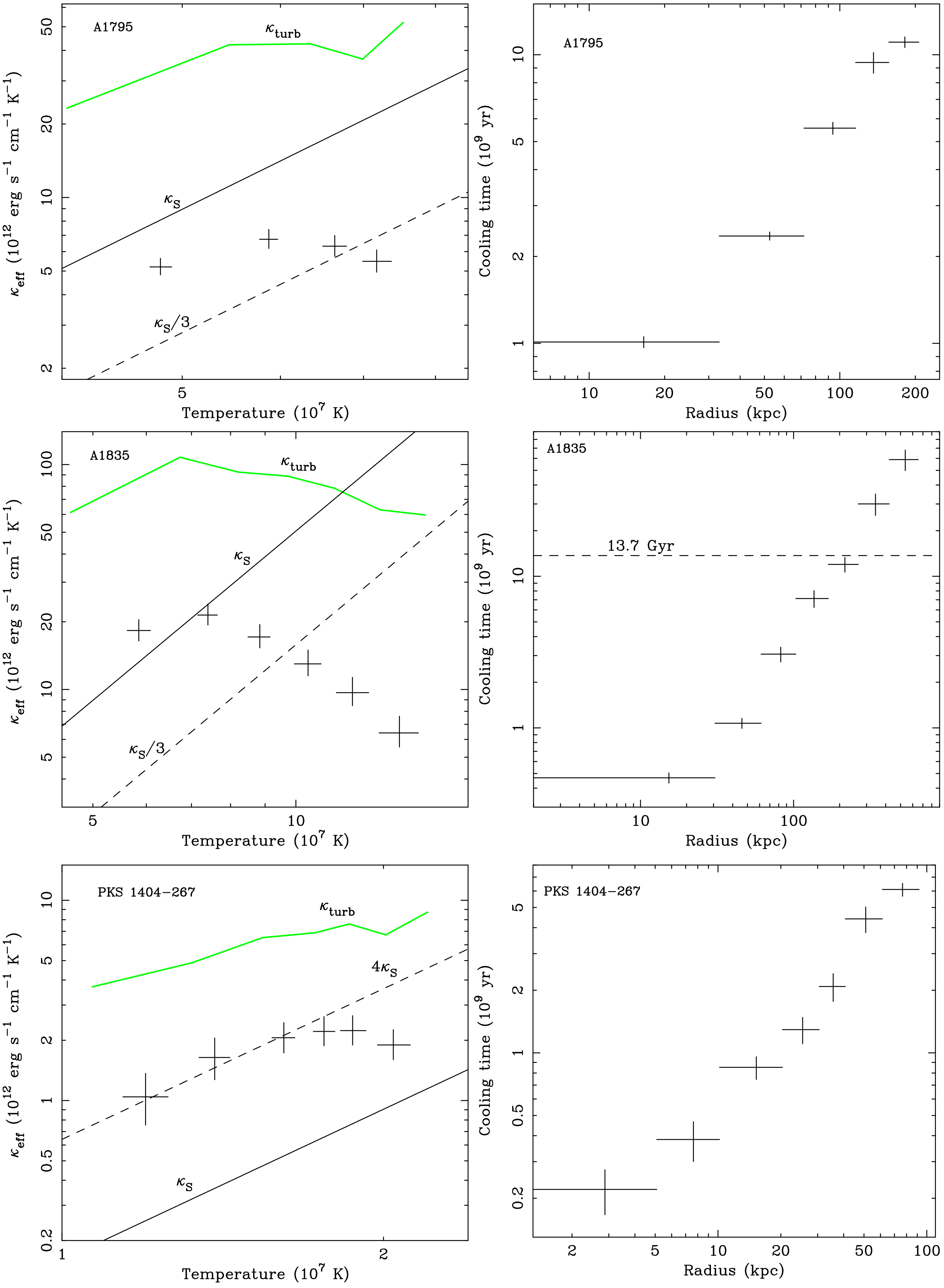
A1795
κturb
κS
κS/3
κeff (10^12 erg s^-1 cm^-1 K^-1)
50
20
10
5
2
5
Temperature (10^7 K)
A1795
Cooling time (10^9 yr)
10
5
2
1
10
20
50
100
200
Radius (kpc)
A1835
κturb
κS
κS/3
κeff (10^12 erg s^-1 cm^-1 K^-1)
100
50
20
10
5
5
10
Temperature (10^7 K)
A1835
13.7 Gyr
Cooling time (10^9 yr)
10
1
10
100
Radius (kpc)
PKS 1404-267
κturb
4κS
κS
κeff (10^12 erg s^-1 cm^-1 K^-1)
10
5
2
1
0.5
0.2
1
2
Temperature (10^7 K)
PKS 1404-267
Cooling time (10^9 yr)
5
2
1
0.5
0.2
2
5
10
20
50
100
Radius (kpc)

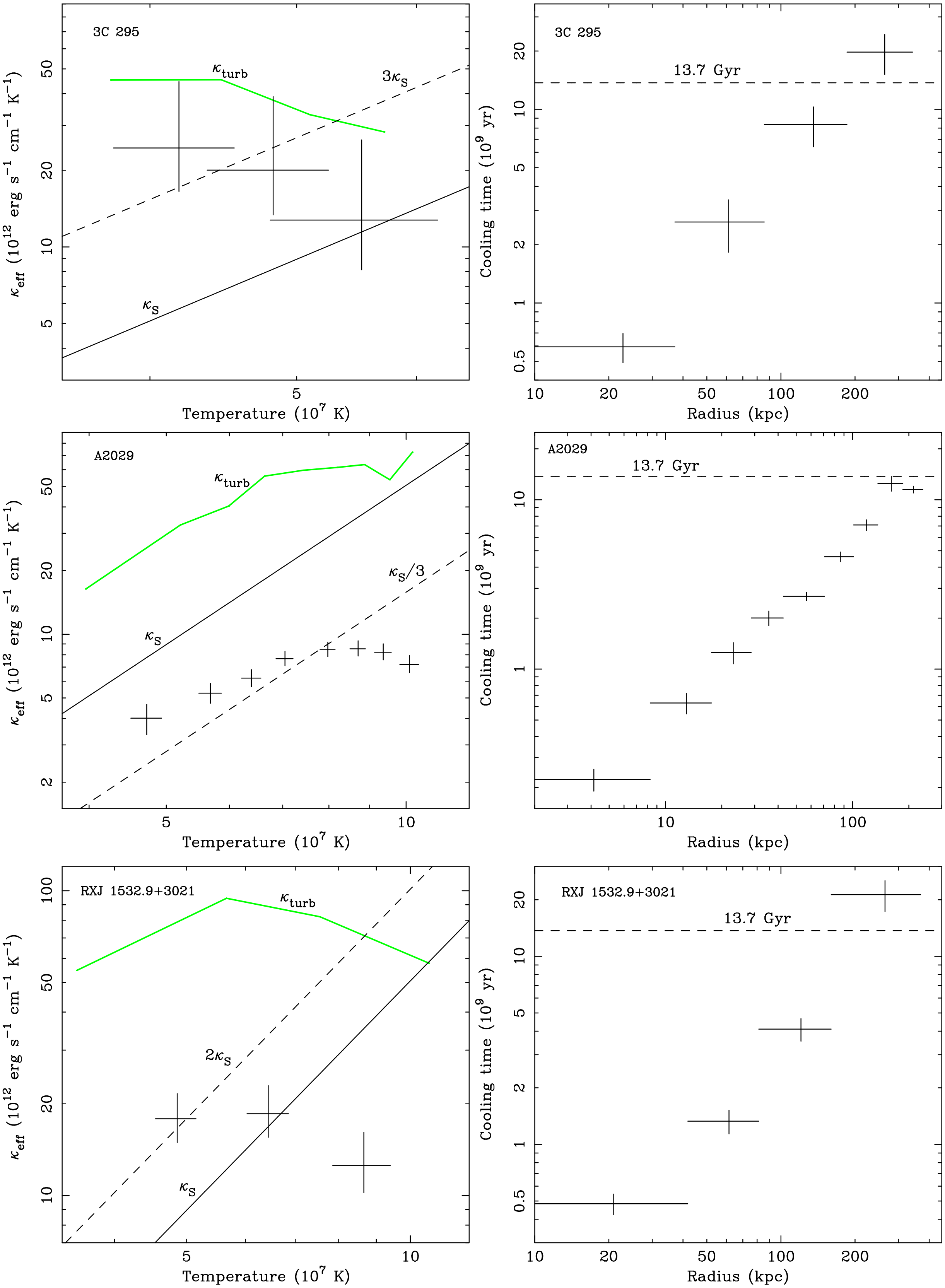
3C 295
κturb
3κS
κS
κeff (10^12 erg s^-1 cm^-1 K^-1)
Temperature (10^7 K)
5 10 20 50
5
3C 295
13.7 Gyr
Cooling time (10^9 yr)
Radius (kpc)
0.5 1 2 5 10 20
10 20 50 100 200
A2029
κturb
κS
κS/3
2 5 10 20 50
5 10
A2029
13.7 Gyr
1 10
10 100
RXJ 1532.9+3021
κturb
2κS
κS
10 20 50 100
5 10
RXJ 1532.9+3021
13.7 Gyr
0.5 1 2 5 10 20
10 20 50 100 200

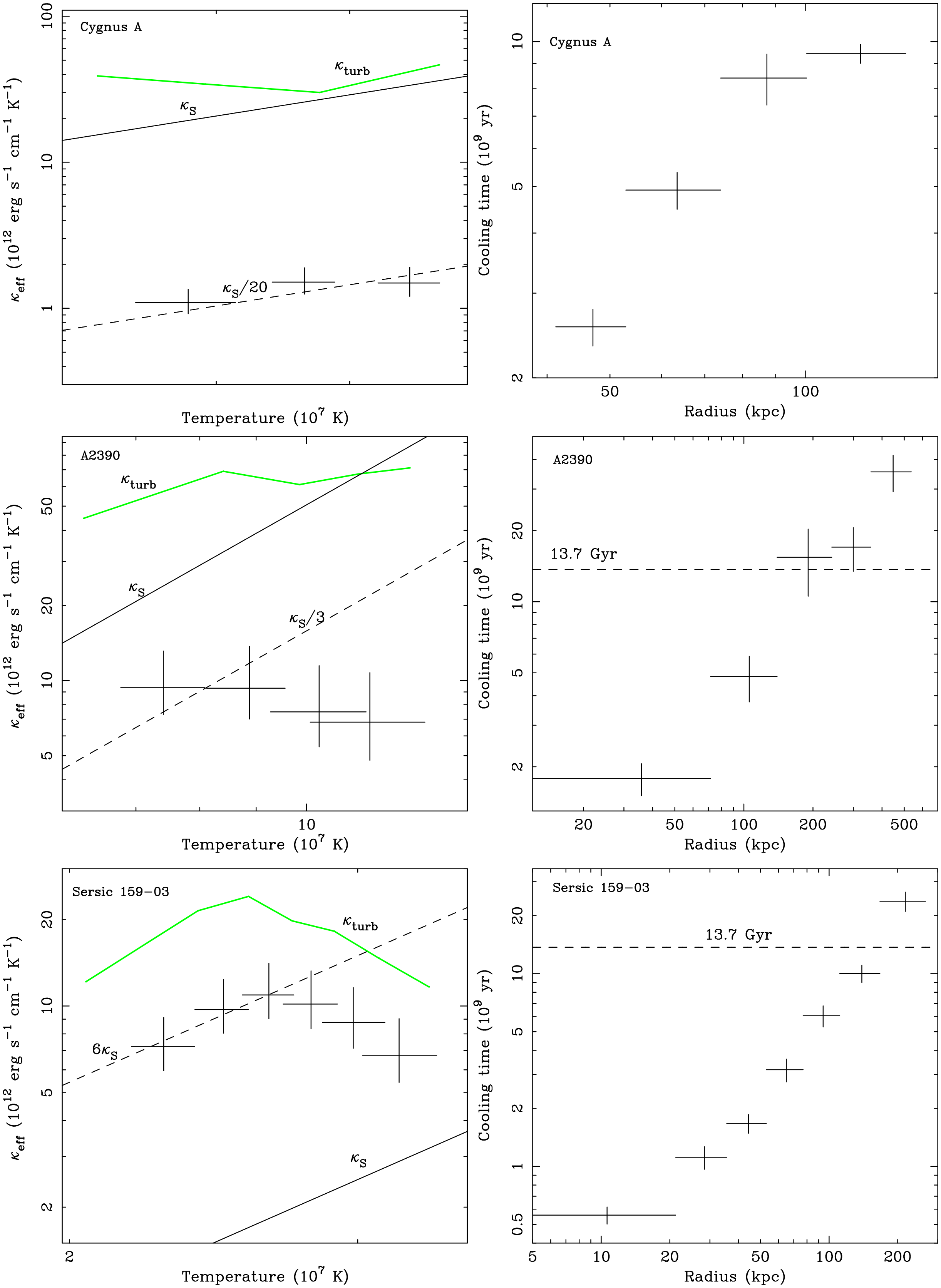
Cygnus A
$\kappa_{\rm turb}$
$\kappa_{\rm S}$
$\kappa_{\rm S}/20$
$\kappa_{\rm eff}$ (10^{12} erg s^{-1} cm^{-1} K^{-1})
100
10
1
Temperature (10^7 K)
Cygnus A
Cooling time (10^9 yr)
10
5
2
50
100
Radius (kpc)
A2390
$\kappa_{\rm turb}$
$\kappa_{\rm S}$
$\kappa_{\rm S}/3$
$\kappa_{\rm eff}$ (10^{12} erg s^{-1} cm^{-1} K^{-1})
50
20
10
5
10
Temperature (10^7 K)
A2390
13.7 Gyr
Cooling time (10^9 yr)
20
10
5
2
20
50
100
200
500
Radius (kpc)
Sersic 159-03
$\kappa_{\rm turb}$
$6\kappa_{\rm S}$
$\kappa_{\rm S}$
$\kappa_{\rm eff}$ (10^{12} erg s^{-1} cm^{-1} K^{-1})
20
10
5
2
2
Temperature (10^7 K)
Sersic 159-03
13.7 Gyr
Cooling time (10^9 yr)
20
10
5
2
1
0.5
5
10
20
50
100
200
Radius (kpc)

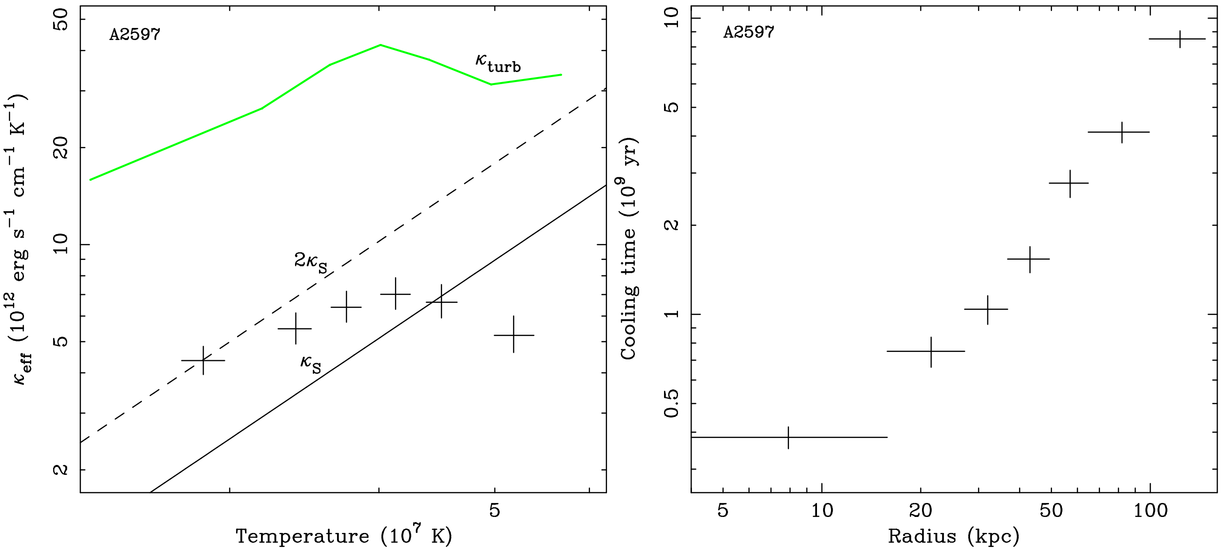

Figure 8. Effective conductivity profiles (left) and cooling times (right) for each cluster. The effective conductivity at the outer boundary of each shell can be compared with the cooling time within that shell. $\kappa_{\rm S}$ and $\kappa_{\rm turb}$ are the Spitzer and turbulent conductivities, respectively. The age of the Universe is 13.7 Gyr for the cosmology used in this paper.